3 TRAJECTORY-PLANNING THROUGH INTERPOLATION BY OVERLAPPING CUBIC ARCS AND CUBIC SPLINES

3.1 Basic interpolation problem in trajectory planning

Given:

(i) a set of nodal points $\{P_i = (x_i, y_i), i = 0,1,...,N\}$ along a general curve C to be followed by a working point (wp) from P_0 to P_N as shown in Figure 3.1,

(ii) prescribed tangential speeds of wp, $\dot{s}_0$ and $\dot{s}_N$ at P_0 and P_N respectively,

(iii) either prescribed tangential acceleration $\ddot{s}_0$ at P_0 *or* $\ddot{s}_N$ at P_N of wp, and

(iv) $\frac{dy}{dx}$ at both P_0 and P_N.

Then it is required to *determine*:

(a) an acceptable time interval $[0,T]$ during which the curve is executed,

(b) time parametric curves $X(t)$ and $Y(t)$, $t \in [0,T]$ that interpolate the nodal points (x_i, y_i), and

(c) continuous time parametric curves for velocities $\dot{X}(t)$ and $\dot{Y}(t)$ as well as for the accelerations $\ddot{X}(t)$ and $\ddot{Y}(t)$, $t \in [0,T]$.

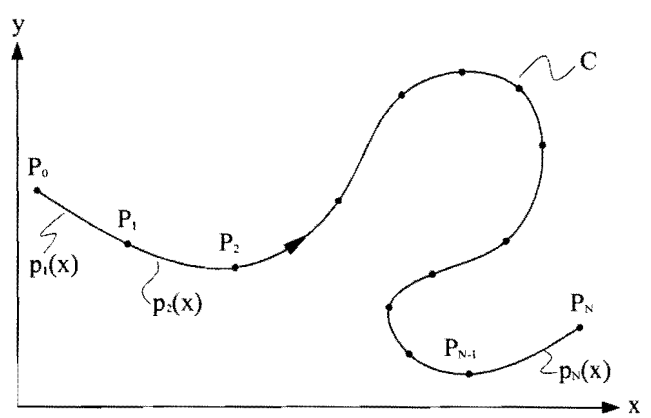

Figure 3.1: Basic interpolation problem.

Without loss in generality consider the case in (iii) where $\ddot{s}_N$ is known at P_N. Objectives (a), (b) and (c) may then be achieved by following the procedure outlined in the following subsections.

3.1.1 Determination of time parametric intervals

In order to achieve objective (a) stipulated above, the first task is to determine the total path length S from P_0 to P_N. This is done as follows: for each arc (x_{i-1}, y_{i-1}) to (x_i, y_i), $i = 1,2,...,N$, determine the corresponding path length s_i. Firstly determine a cubic interpolating polynomial approximation $p_i(x)$ over each arc interval, i.e. $y(x) \approx p_i(x)$, $x \in [x_{i-1}, x_i]$ (or $x(y) \approx p_i(y)$, $y \in [y_{i-1}, y_i]$ depending on what is the most convenient).

3.1.1.1 Determination of interpolating and overlapping cubic arcs

It is assumed that for any three consecutive nodal points (nodes) P_{i-1}, P_i and P_{i+1}, $i = 1,2,...,N-1$ in the given set of nodal points $\{P_i = (x_i, y_i), i = 0,1,...,N\}$, at least *one* of the following conditions must hold:

Condition 1(a):	$x_{i+1} > x_i > x_{i-1}$
Condition 1(b):	$x_{i+1} < x_i < x_{i-1}$
Condition 2(a):	$y_{i+1} > y_i > y_{i-1}$
Condition 2(b):	$y_{i+1} < y_i < y_{i-1}$

Table 3.1

In the event of non-compliance with all four the above conditions, the set of nodal points is considered insufficient since it implies that the section of the curve, represented by the three nodes that do not satisfy any of the conditions, cannot be expressed in the form where one of the coordinate variables is a unique valued function of the other. An extreme example of this non-uniqueness is depicted in Figure 3.2 which shows a complete curve C represented by the three nodes P_0, P_1 and P_2.

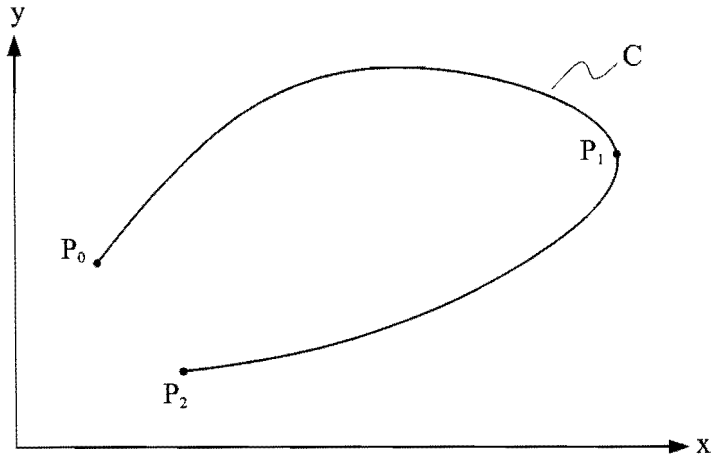

Figure 3.2: Insufficient set of nodal points.

Clearly $x_2 < x_1$ while $x_1 > x_0$, violating both conditions 1(a) and 1(b), and further $y_2 < y_1$ while $y_1 > y_0$, violating both conditions 2(a) and 2(b). This situation can easily be remedied by specifying, for example, two additional nodes, resulting in a set of five nodal points, as shown in Figure 3.3.

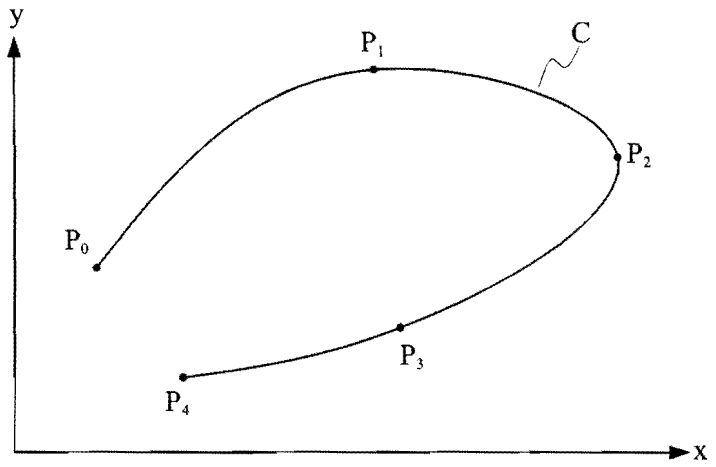

Figure 3.3: Sufficient set of nodal points.

The five nodal points shown in Figure 3.3, $\{P_i = (x_i, y_i), i = 0,1,...,4\}$ may be grouped to form three overlapping triplets of consecutive nodes, i.e.

Triplet 1:	(P_0, P_1, P_2)	$x_2 > x_1 > x_0$ (*satisfying* condition 1(a)) $y_2 < y_1$ and $y_1 > y_0$ (*violating* conditions 2(a) and 2(b))
Triplet 2:	(P_1, P_2, P_3)	$x_3 < x_2$ and $x_2 > x_1$ (*violating* conditions 1(a) and 1(b)) $y_3 < y_2 < y_1$ (*satisfying* condition 2(b))
Triplet 3:	(P_2, P_3, P_4)	$x_4 < x_3 < x_2$ (*satisfying* condition 1(b)) $y_4 < y_3 < y_2$ (*satisfying* condition 2(b))

Table 3.2

Curve C shown in Figure 3.3 may now be approximated by four (in general N) overlapping interpolating arcs shown separately in Figures 3.4, 3.5 and 3.6. Along each arc one variable may be expressed as a *unique* function of the other depending on which condition in Table 3.1 is satisfied. In particular it may be desired to represent each arc by a cubic polynomial interpolating function.

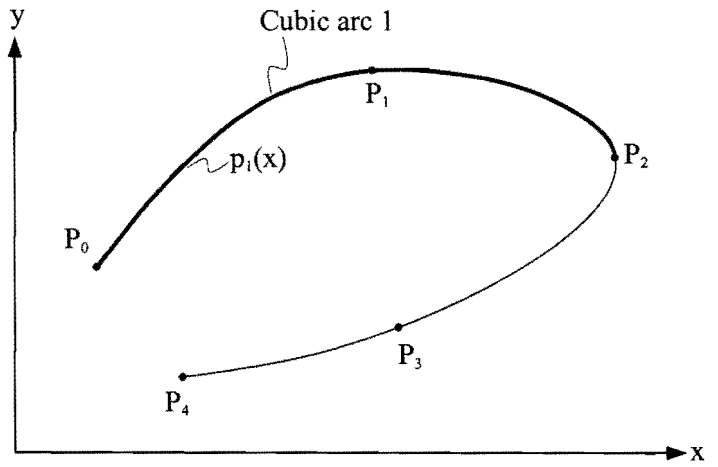

Figure 3.4: Cubic arc 1.

It follows by inspection that arc 1 in Figure 3.4, passing through the three nodes of triplet 1, may be represented by a unique valued function of x (see Tables 3.1 and 3.2). In particular it may be expressed as a cubic polynomial in x of the form:

$$p_1(x) = a_1 + b_1(x - x_0) + c_1(x - x_0)^2 + d_1(x - x_0)^3, \; x \in [x_0, x_2] \tag{3.1}$$

The derivative of (3.1) with respect to x is given by

$$\frac{d}{dx}p_1(x) = b_1 + 2c_1(x - x_0) + 3d_1(x - x_0)^2, \; x \in [x_0, x_2] \tag{3.2}$$

The four unknown coefficients of the cubic interpolating polynomial (a_1, b_1, c_1 and d_1) may be uniquely determined by utilizing the initial known gradient, i.e. $\frac{dy}{dx}$ at P_0 (see given data (iv), at the start of Section 3.1), as well as the three nodal points of triplet 1. More specifically substituting each of the three nodal points of triplet 1 into equation (3.1), results in three independent equations:

$$y_0 = p_1(x_0) = a_1 \tag{3.3}$$

$$y_1 = p_1(x_1) = a_1 + b_1(x_1 - x_0) + c_1(x_1 - x_0)^2 + d_1(x_1 - x_0)^3 \tag{3.4}$$

$$y_2 = p_1(x_2) = a_1 + b_1(x_2 - x_0) + c_1(x_2 - x_0)^2 + d_1(x_2 - x_0)^3 \tag{3.5}$$

The fourth independent equation follows from substituting the initial gradient $\frac{dy}{dx}$ at P_0 $\left(\left.\frac{dy}{dx}\right|_{P_0}\right)$ into equation (3.2):

$$\left.\frac{dy}{dx}\right|_{P_0} = \frac{dy(x_0)}{dx} \approx \frac{d}{dx}p_1(x_0) = b_1 \tag{3.6}$$

With a_1 and b_1 known from expressions (3.3) and (3.6) respectively, one may solve for c_1 and d_1 using expressions (3.4) and (3.5):

$$\text{from (3.4): } c_1 = \frac{y_1 - a_1 - b_1(x_1 - x_0)}{(x_1 - x_0)^2} - d_1(x_1 - x_0)$$

$$\text{or } c_1 = e_1 - d_1(x_1 - x_0)$$

$$\text{where } e_1 = \frac{y_1 - a_1 - b_1(x_1 - x_0)}{(x_1 - x_0)^2}, \text{ and substituting the expression for } c_1$$

$$\text{into (3.5): } y_2 = a_1 + b_1(x_2 - x_0) + (e_1 - d_1(x_1 - x_0))(x_2 - x_0)^2 + d_1(x_2 - x_0)^3$$

$$\text{and therefore } d_1 = \frac{y_2 - a_1 - b_1(x_2 - x_0) - e_1(x_2 - x_0)^2}{(x_2 - x_0)^3 - (x_1 - x_0)(x_2 - x_0)^2}$$

It is proposed here that the cubic interpolating polynomial $p_1(x)$ constructed in this manner be called a clamped three-order interpolating cubic arc, or simply a *C-3 node cubic arc*.

Although cubic arc 1 interpolates through points P_0, P_1 and P_2 and is thus valid over the interval $[x_0, x_2]$, it will only be used to represent the cubic polynomial function over the first interval $[x_0, x_1]$. Cubic arc 1 is forced through the three nodes of triplet 1 (see Table 3.1) with only the initial gradient $\left(\left.\frac{dy}{dx}\right|_{P_0}\right)$ being enforced. The approximation $p_1(x)$ is therefore expected to deteriorate in gradient accuracy in the vicinity of node P_2 and this is the reason why it will only be used over $[x_0, x_1]$. To obtain a more reliable approximation between nodes P_1 and P_2 an overlapping strategy is employed to avoid the accumulation of excessive gradient approximation errors, which will result in increasingly inaccurate fitted cubic arcs.

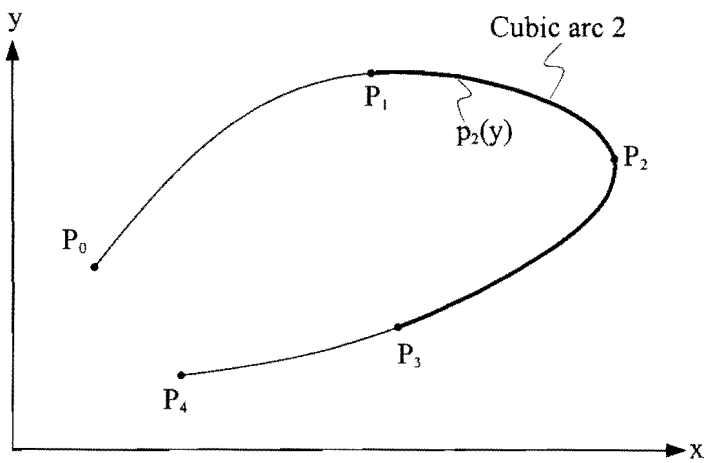

Figure 3.5: Cubic arc 2.

The cubic arc 2 passing through the three nodes of triplet 2, (see Figure 3.5) is also represented by a cubic polynomial function this time of y (see also Table 3.1 and Table 3.2). This function is formally expressed as

$$p_2(y) = a_2 + b_2(y - y_1) + c_2(y - y_1)^2 + d_2(y - y_1)^3,\ y \in [y_1, y_3] \tag{3.7}$$

The derivative of (3.7) with respect to y is

$$\frac{d}{dy}p_2(y) = b_2 + 2c_2(y - y_1) + 3d_2(y - y_1) \tag{3.8}$$

Again the initial gradient of cubic arc 2 at P_1 $\left(\left.\frac{dx}{dy}\right|_{P_1}\right)$ is required together with the three nodes of triplet 2 to calculate the four unknown coefficients (a_2, b_2, c_2 and d_2) of polynomial (3.7). Here, at the start of arc 2 (as for the subsequent arcs) the value of the gradient is not explicitly prescribed and is therefore unknown. However, once the four unknown coefficients of the previous cubic arc 1 have been determined, equation (3.2) provides an approximation to the required gradient at P_1, i.e.

$$\left.\frac{dy}{dx}\right|_{P_1} = \frac{dy(x_1)}{dx} \approx \frac{d}{dx}p_1(x_1) = b_1 + 2c_1(x_1 - x_0) + 3d_1(x_1 - x_0)^2 \tag{3.9}$$

Thus in computing the coefficients of approximating arc 2 the condition $\left.\frac{dx}{dy}\right|_{P_1} = \left[\frac{dp_1(x_1)}{dx}\right]^{-1}$ is used.

Polynomial $p_2(x)$ will only be used to describe the arc between nodes P_1 and P_2.

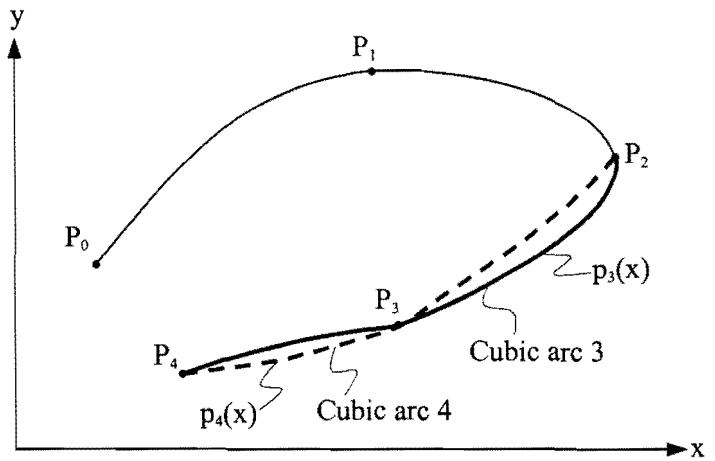

Figure 3.6: Cubic arcs 3 and 4.

Cubic arc 3 passing through the three nodes of triplet 3 (see Figure 3.6) is different to the previous arcs in that both conditions 1(b) and 2(b) are satisfied (see Table 3.1 and Table 3.2). This implies that cubic arc 3 can be expressed as a cubic polynomial function of either x or y and a choice has to be made. If this situation occurs, only one of the following two conditions will be satisfied:

Condition 3(a):	$\lvert x_{i+1} - x_{i-1}\rvert \geq \lvert y_{i+1} - y_{i-1}\rvert$
Condition 3(b):	$\lvert x_{i+1} - x_{i-1}\rvert < \lvert y_{i+1} - y_{i-1}\rvert$

Table 3.3

For the case depicted in Figure 3.6, cubic arc 3 satisfies condition 3(a) in Table 3.3, and it is therefore clearly preferable to express the arc as a cubic polynomial function of x:

$$p_3(x) = a_3 + b_3(x-x_2) + c_3(x-x_2)^2 + d_3(x-x_2)^3,\ x \in [x_2, x_4] \qquad (3.10)$$

The unknown coefficients of cubic polynomial (3.10) are determined in a similar manner to those of cubic arc 2 (equation (3.7)), with the initial gradient at P_2 taken as $\left.\frac{dy}{dx}\right|_{P_2} = \left[\frac{dp_2(y_2)}{dy}\right]^{-1}$. Again $p_3(x)$ will only be used over the first interpolating interval, i.e., between nodes P_2 and P_3 (Figure 3.6).

Having determined cubic arc 3, it remains to find a suitable cubic interpolating polynomial function $p_4(x)$, $x \in [x_3, x_4]$, which is to represent the final interval P_3 to P_4 of the total curve under consideration.

The overlapping strategy may be continued for the final part of the curve by fitting a cubic arc through nodes P_4, P_3 and P_2, and utilizing the given gradient at P_4 (see given data (iv) at the beginning of Section 3.1). The polynomial has the form

$$p_4(x) = a_4 + b_4(x-x_4) + c_4(x-x_4)^2 + d_4(x-x_4)^3,\ x \in [x_4, x_2] \qquad (3.11)$$

The derivative of (3.11) with respect to x is

$$\frac{d}{dx}p_4(x) = b_4 + 2c_4(x-x_4) + 3d_4(x-x_4)^2,\ x \in [x_4, x_2] \qquad (3.12)$$

With the given final gradient $\frac{dy}{dx}$ at P_4 and interpolating through the three nodes P_4, P_3 and P_2, four independent equations in the unknown coefficients follow from expressions (3.11) and (3.12) as before. These equations may be simultaneously solved to give a_4, b_4, c_4 and d_4. The resultant interpolating polynomial $p_4(x)$, representing arc 4 and to be used over the final interval between nodes P_3 and P_4, is also indicated in Figure 3.6.

The following truth table shows how the different conditions listed in Table 3.1 and Table 3.3 determine the dependent variable for a specific arc. The rows show different combinations of satisfied and violated conditions, where a 1 indicates that a specific condition is satisfied and a 0 that it is violated.

Condition 1(a)	Condition 1(b)	Condition 2(a)	Condition 2(b)	Condition 3(a)	Condition 3(b)	Dependent variable
1	0	0	0			x
0	1	0	0			x
0	0	1	0			y
0	0	0	1			y
1	0	1	0	1	0	x
				0	1	y
1	0	0	1	1	0	x
				0	1	y
0	1	1	0	1	0	x
				0	1	y
0	1	0	1	1	0	x
				0	1	y

Table 3.4

Here, for illustrative purposes, the presentation of the overlapping cubic arc methodology for constructing an approximation to a curve defined by nodal points $P_0, P_1, ..., P_N$, has been restricted to the case $N = 4$. The extension of the method to the more general case where N may be larger than 4 is clear and obvious.

3.1.1.2 Computation of total path length S

With $p_i(x)$ (or $p_i(y)$) representing the approximation to the curve to be used over $[x_{i-1}, x_i]$ known, the corresponding curve length s_i may be obtained by integration. From the differential relationship $ds^2 = dx^2 + dy^2$ it follows that $ds = \sqrt{1 + (\frac{dy}{dx})^2}\,dx$ and therefore the curve length s_i is given by

$$s_i = \int_{x_{i-1}}^{x_i} \sqrt{1 + (\tfrac{d}{dx} p_i(x))^2}\,dx = \int_a^b f(x)dx$$

$$\text{with } a = x_{i-1},\ b = x_i \text{ and } f(x) = \sqrt{1 + [b_i + 2c_i(x - x_{i-1}) + 3d_i(x - x_{i-1})^2]^2}$$

$$\text{for each } i = 1,2,...,N$$

It is convenient to do the integration numerically by using the composite Simpson's rule for n subintervals [55]:

$$\int_a^b f(x)dx \approx \frac{h}{3}\left[f(a) + 2\sum_{j=1}^{(n/2)-1} f(x_{2j}) + 4\sum_{j=1}^{(n/2)} f(x_{2j-1}) + f(b) \right] \qquad (3.13)$$

where n is even, $h = \dfrac{(b-a)}{n}$, and $x_k = a + kh$ for $k = 0,1,...,n$

The total path length S of curve C is then given by

$$S = \sum_{i=1}^{N} s_i \tag{3.14}$$

3.1.1.3 Dependence of curve length on parameter t

Assume that the distance s of the working point (wp) along the curve is represented by a cubic polynomial in time t of the form:

$$s(t) = a_s + b_s t + c_s t^2 + d_s t^3,\ t \in [0,T] \tag{3.15}$$

Expression (3.15) is associated with a known initial curve length $s(0) = s_0$ (usually $s_0 = 0$), a known initial tangential speed $\dot{s}(0) = v_0$ (usually $v_0 = 0$), as well as a known final curve length $s(T) = S$ (usually found via expression (3.14) above).

For the time being, assume that a gradual increase in tangential speed is required over the time interval $t \in [0,T]$, such that a specified tangential speed v^* is attained at time T, i.e. $\dot{s}(T) = v^*$. The time derivative of (3.15), representing the tangential speed over the total path is

$$\dot{s}(t) = b_s + 2c_s t + 3d_s t^2,\ t \in [0,T] \tag{3.16}$$

The acceleration over the total path may be obtained from the time derivative of (3.16):

$$\ddot{s}(t) = 2c_s + 6d_s t,\ t \in [0,T] \tag{3.17}$$

It is further required that the magnitude of the final tangential acceleration has to be zero, i.e. $\ddot{s}(T) = 0$.

Now, with $s(0) = s_0$, $s(T) = S$, $\dot{s}(0) = v_0$, $\dot{s}(T) = v^*$ and $\ddot{s}(T) = 0$ known, one may solve for a_s, b_s, c_s, d_s and T as follows:

$$s(0) = a_s = s_0$$

$$\dot{s}(0) = b_s = v_0$$

$$s(T) = S = a_s + b_s T + c_s T^2 + d_s T^3 \tag{3.18}$$

$$\dot{s}(T) = v^* = b_s + 2c_s T + 3d_s T^2 \tag{3.19}$$

$$\ddot{s}(T) = 0 = 2c_s + 6d_s T \tag{3.20}$$

$$\text{from (3.20): } c_s = -3d_s T \tag{3.21}$$

and substituting (3.21) into (3.19): $v^* = v_0 - 3d_s T^2$, from which it follows that

$$d_s = \frac{v_0 - v^*}{3T^2} \tag{3.22}$$

$$\text{Substituting (3.22) into (3.21): } c_s = \frac{v^* - v_0}{T} \tag{3.23}$$

and substituting (3.22) and (3.23) into (3.18): $S = s_0 + T\left(\frac{v_0}{3} + \frac{2v^*}{3}\right)$ from which it finally follows that

$$T = \frac{3(S - s_0)}{v_0 + 2v^*} \tag{3.24}$$

Note that if the initial time instant $t_0 \neq 0$, the corresponding polynomial $s(t)$ can readily be obtained by the simple replacement of T by $T - t_0$ in expressions (3.18) - (3.24) and the corresponding replacement of t by $t - t_0$ in expressions (3.17) - (3.19).

For each node $P_i = (x_i, y_i)$, $i = 0,1,...,N$ the total path length up to the specific node may be determined from (3.14):

$$S_i = \sum_{j=1}^{i} s_j, \; i = 0,1,...,N \tag{3.25}$$

Further, with S_i, $i = 1,2,...,N-1$ known, the Newton-Raphson iterative method may be used to solve for the corresponding nodal times t_i, $i = 1,2,...,N-1$ [55]. This well-known and powerful numerical method solves for the root of a non-linear equation of the form $f(x) = 0$ via the iterative scheme:

$$x^{(j)} = \frac{x^{(j-1)} - f(x^{(j-1)})}{\left[\frac{df(x^{(j-1)})}{dx}\right]}, \; j = 1,2,...$$

where an initial estimate $x^{(0)}$ is given.

To solve for a specific t_i corresponding to distance S_i, requires the solution of the non-linear equation

$$f(t_i) = s(t_i) - S_i = 0$$

where from (3.15): $s(t_i) = a_s + b_s t_i + c_s t_i^2 + d_s t_i^3$, and thus, more explicitly, the equation to be solved becomes

$$f(t_i) = a_s + b_s t_i + c_s t_i^2 + d_s t_i^3 - S_i = 0$$

An equation corresponding to the above, is to be solved for each $i = 1,2,...,N-1$.

Since $t_N = T$ is known from (3.24), good initial approximations for t_i, $i = 1,2,...,N-1$ may be found:

$$t_i^{(0)} = i\left(\frac{T}{N}\right), \; i = 1,2,...,N-1$$

Starting with an initial approximate root given by the above, the Newton-Raphson method generates, for each *i*, a sequence of approximations $\{t_i^{(j)}, j = 0,1,2,...\}$:

$$t_i^{(j)} = t_i^{(j-1)} - \frac{f(t_i^{(j-1)})}{\left[\frac{df(t_i^{(j-1)})}{dt_i}\right]},\ j = 1,2,...$$

The iteration continues until convergence is obtained. In practice, with a tolerance $\varepsilon > 0$ specified, the Newton-Raphson iteration continues for each i until one of the following convergence criteria is met:

$$\left|t_i^{(j)} - t_i^{(j-1)}\right| < \varepsilon$$

$$\frac{\left|t_i^{(j)} - t_i^{(j-1)}\right|}{t_i^{(j)}} < \varepsilon,\ t_i^{(j)} \neq 0$$

$$\text{or } f(t_i^{(j)}) < \varepsilon$$

3.1.2 Cubic spline representations for X(t) and Y(t)

With the time interval $[0,T]$ during which the curve is executed determined (see objective (a) Section 3.1), and the nodal times t_i, $i = 1,2,...,N-1$ known, time parametric curves $X(t)$, and $Y(t)$, $t \in [0,T]$ interpolating the nodal points (x_i, y_i) (see objective (b) Section 3.1), can be determined.

Since a unique time instant $t_i \in [0,T]$ is associated with each nodal point (x_i, y_i), $i = 0,1,...,N$ and since $0 = t_0 < t_1 < ... < t_N = T$, separate *cubic spline interpolations* $X(t)$ and $Y(t)$ may be fitted to the respective nodal point sets, (x_i, t_i) and (y_i, t_i).

According to Burden and Faires [55] cubic spline interpolation, which fits cubic polynomials between each successive pair of nodes, is the most common piecewise polynomial approximation. Based on their definition, the cubic spline interpolant $X(t)$, is a function that satisfies the following conditions:

$X(t)$ is a cubic polynomial, denoted $X_i(t)$, on subinterval $[t_i, t_{i+1}]$ for each $i = 0,1,...,N-1$

$X(t_i) = x_i$ for each $i = 0,1,...,N$

$X_{i+1}(t_{i+1}) = X_i(t_{i+1})$ for each $i = 0,1,...,N-2$

$\dot{X}_{i+1}(t_{i+1}) = \dot{X}_i(t_{i+1})$ for each $i = 0,1,...,N-2$

$\ddot{X}_{i+1}(t_{i+1}) = \ddot{X}_i(t_{i+1})$ for each $i = 0,1,...,N-2$

One of the following set of boundary conditions is satisfied:

$\ddot{X}(t_0) = \ddot{X}_i(t_N) = 0$ (free or natural boundary)

or $\dot{X}(t_0) = \dot{x}_0$ and $\dot{X}(t_N) = \dot{x}_N$ (clamped boundary)

When the free boundary conditions are prescribed, the spline is called a natural spline, and its form approximates the shape that a long flexible rod would assume if forced to go through each of the nodal points.

For the interpolants X(t) and Y(t) to be constructed here, however, clamped boundary conditions are used, since they contain more information about the respective functions, and therefore lead to more accurate approximations.

Assume for the moment that the derivatives at the end points ($\dot{x}_0$ and $\dot{x}_N$) are accurately known. To construct the cubic spline interpolant for x as a function of t, the conditions listed above are applied to the cubic polynomials of the following form:

$$X_i(t) = a_{Xi} + b_{Xi}(t-t_i) + c_{Xi}(t-t_i)^2 + d_{Xi}(t-t_i)^3,\ i = 0,1,...,N-1 \qquad (3.26)$$

The unknown coefficients a_{Xi}, b_{Xi}, c_{Xi} and d_{Xi}, $i = 0,1,...,N-1$, may easily be determined as shown in [55].

If not explicitly known, the initial derivative $\dot{x}_0$ may be accurately approximated using Taylor expansions for x_1, x_2, x_3 and x_4 about t_0:

$$x_1 = x_0 + \Delta t_1\dot{x}_0 + \frac{(\Delta t_1)^2}{2!}\ddot{x}_0 + \frac{(\Delta t_1)^3}{3!}\dddot{x}_0 + \frac{(\Delta t_1)^4}{4!}\ddddot{x}_0 + O(\Delta t_1)^5$$

$$x_2 = x_0 + \Delta t_2\dot{x}_0 + \frac{(\Delta t_2)^2}{2!}\ddot{x}_0 + \frac{(\Delta t_2)^3}{3!}\dddot{x}_0 + \frac{(\Delta t_2)^4}{4!}\ddddot{x}_0 + O(\Delta t_2)^5$$

$$x_3 = x_0 + \Delta t_3\dot{x}_0 + \frac{(\Delta t_3)^2}{2!}\ddot{x}_0 + \frac{(\Delta t_3)^3}{3!}\dddot{x}_0 + \frac{(\Delta t_3)^4}{4!}\ddddot{x}_0 + O(\Delta t_3)^5$$

$$x_4 = x_0 + \Delta t_4\dot{x}_0 + \frac{(\Delta t_4)^2}{2!}\ddot{x}_0 + \frac{(\Delta t_4)^3}{3!}\dddot{x}_0 + \frac{(\Delta t_4)^4}{4!}\ddddot{x}_0 + O(\Delta t_4)^5$$

where x_i corresponds to $x(t_i)$ and $\Delta t_i = t_i - t_0$, $i = 1,2,3,4$. Ignoring the higher order terms in the above expressions leads to the following set of linear equations:

$$\begin{bmatrix} x_1 - x_0 \\ x_2 - x_0 \\ x_3 - x_0 \\ x_4 - x_0 \end{bmatrix} = \begin{bmatrix} \Delta t_1 & \frac{(\Delta t_1)^2}{2} & \frac{(\Delta t_1)^3}{6} & \frac{(\Delta t_1)^4}{24} \\ \Delta t_2 & \frac{(\Delta t_2)^2}{2} & \frac{(\Delta t_2)^3}{6} & \frac{(\Delta t_2)^4}{24} \\ \Delta t_3 & \frac{(\Delta t_3)^2}{2} & \frac{(\Delta t_3)^3}{6} & \frac{(\Delta t_3)^4}{24} \\ \Delta t_4 & \frac{(\Delta t_4)^2}{2} & \frac{(\Delta t_4)^3}{6} & \frac{(\Delta t_4)^4}{24} \end{bmatrix} \begin{bmatrix} \dot{x}_0 \\ \ddot{x}_0 \\ \dddot{x}_0 \\ \ddddot{x}_0 \end{bmatrix} \qquad (3.27)$$

Expression (3.27) is a linear system of the form $\mathbf{Ax} = \mathbf{b}$, and can be solved directly using a scheme such as LU-factorization [55]. The solution vector $\mathbf{x}$ contains the sought after initial derivative $\dot{x}_0$.

The final derivative $\dot{x}_N$ may be obtained in a similar manner, where the set of linear equations in matrix form is given by:

$$\begin{bmatrix} x_{N-1}-x_N \\ x_{N-2}-x_N \\ x_{N-3}-x_N \\ x_{N-4}-x_N \end{bmatrix} = \begin{bmatrix} -\Delta t_1 & \frac{(\Delta t_1)^2}{2} & -\frac{(\Delta t_1)^3}{6} & \frac{(\Delta t_1)^4}{24} \\ -\Delta t_2 & \frac{(\Delta t_2)^2}{2} & -\frac{(\Delta t_2)^3}{6} & \frac{(\Delta t_2)^4}{24} \\ -\Delta t_3 & \frac{(\Delta t_3)^2}{2} & -\frac{(\Delta t_3)^3}{6} & \frac{(\Delta t_3)^4}{24} \\ -\Delta t_4 & \frac{(\Delta t_4)^2}{2} & -\frac{(\Delta t_4)^3}{6} & \frac{(\Delta t_4)^4}{24} \end{bmatrix} \begin{bmatrix} \dot{x}_N \\ \ddot{x}_N \\ \dddot{x}_N \\ \ddddot{x}_N \end{bmatrix} \tag{3.28}$$

with $\Delta t_i = t_N - t_{N-i}$, $i = 1,2,3,4$.

The advantage of using a cubic spline interpolation for $X(t)$, $t \in [0,T]$ is that each constituent cubic polynomial $X_i(t)$ involves four coefficients, so there is sufficient flexibility in the cubic spline procedure to ensure that the interpolant is not only continuously differentiable, but also has a continuous second derivative over the whole interval $[0,T]$ (see [55]).

Once a_{Xi}, b_{Xi}, c_{Xi}, and d_{Xi}, $i = 0,1,...,N-1$ (see (3.26)) are determined, $\dot{X}(t)$ and $\ddot{X}(t)$ are given by:

$$\dot{X}_i(t) = b_{Xi} + 2c_{Xi}(t-t_i) + 3d_{Xi}(t-t_i)^2, \; i = 0,1,...,N-1 \tag{3.29}$$

$$\ddot{X}_i(t) = 2c_{Xi} + 6d_{Xi}(t-t_i), \; i = 0,1,...,N-1 \tag{3.30}$$

which are continuous functions over the interval $[0,T]$ (see objective (c) Section 3.1).

It follows that $Y(t)$, $\dot{Y}(t)$ and $\ddot{Y}(t)$ can be found in a similar manner.

3.2 Practical problem of determining $\frac{dy}{dx}$ at P_0 and P_N

In general the set of given nodal points $\{P_i = (x_i, y_i), i = 0,1,...,N\}$ may represent a curve for which no explicit analytical expression exists, and therefore the exact initial and final gradients ($\frac{dy}{dx}$ at P_0 and P_N) will not be known. In this case approximations to these gradients with respect to x may be determined using Taylor expansions in an analogous manner as done for the time derivatives $\dot{x}_0$ and $\dot{x}_N$ in Section 3.1.2 (see expressions (3.27) and (3.28)).

In Section 3.1.1.1 it is apparent that the nodal points representing a curve must be chosen in such a way that certain conditions are satisfied (see Table 3.1 and Table 3.3). These conditions ensure that each consecutive cubic arc can be expressed as a function of either x or y.

Returning to the illustrative example curve of Figure 3.3, it was shown that 5 nodal points along the curve are adequate in terms of the conditions listed in Table 3.1 and Table 3.3, provided that the exact initial and final gradients are known. However, if the exact values of the initial and final gradients are not known, the nodal points should be specified in such a way that sufficiently *accurate approximations* for these gradients may be calculated.

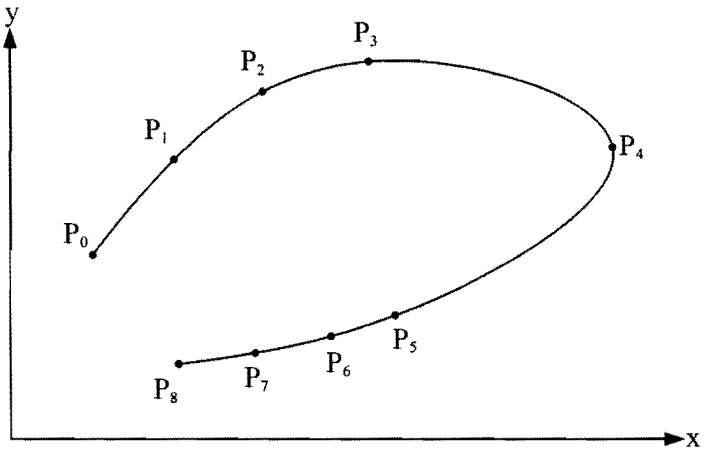

Figure 3.7: Additional nodal points specified.

Figure 3.7 shows the same illustrative example curve, but with four additional nodal points. An approximate value for the initial gradient ($\frac{dy}{dx}$ at P_0, i.e. y'_0) may then be determined using the following Taylor expansions:

$$y_1 = y_0 + \Delta x_1 y'_0 + \frac{(\Delta x_1)^2}{2!} y''_0 + \frac{(\Delta x_1)^3}{3!} y'''_0 + O(\Delta x_1)^4$$

$$y_2 = y_0 + \Delta x_2 y'_0 + \frac{(\Delta x_2)^2}{2!} y''_0 + \frac{(\Delta x_2)^3}{3!} y'''_0 + O(\Delta x_2)^4$$

$$y_3 = y_0 + \Delta x_3 y'_0 + \frac{(\Delta x_3)^2}{2!} y''_0 + \frac{(\Delta x_3)^3}{3!} y'''_0 + O(\Delta x_3)^4$$

with $\Delta x_i = x_i - x_0$, $i = 1,2,3$.

The clustered distribution of nodal points P_0, P_1, P_2 and P_3 shown in Figure 3.7 is justified considering the fact that the fourth order error term in the above Taylor expansions becomes smaller using smaller step sizes Δx_1, Δx_2 and Δx_3. Neglecting these error terms an approximate initial gradient y'_0 is obtained by solving the following linear system:

$$\begin{bmatrix} y_1 - y_0 \\ y_2 - y_0 \\ y_3 - y_0 \end{bmatrix} = \begin{bmatrix} \Delta x_1 & \frac{(\Delta x_1)^2}{4} & \frac{(\Delta x_1)^3}{6} \\ \Delta x_2 & \frac{(\Delta x_2)^2}{4} & \frac{(\Delta x_2)^3}{6} \\ \Delta x_3 & \frac{(\Delta x_3)^2}{4} & \frac{(\Delta x_3)^3}{6} \end{bmatrix} \begin{bmatrix} y'_0 \\ y''_0 \\ y'''_0 \end{bmatrix} \tag{3.31}$$

Similarly, an approximate final gradient y'_N may be obtained by solving the linear system:

$$\begin{bmatrix} y_{N-1} - y_N \\ y_{N-2} - y_N \\ y_{N-3} - y_N \end{bmatrix} = \begin{bmatrix} -\Delta x_1 & \frac{(\Delta x_1)^2}{4} & -\frac{(\Delta x_1)^3}{6} \\ -\Delta x_2 & \frac{(\Delta x_2)^2}{4} & -\frac{(\Delta x_2)^3}{6} \\ -\Delta x_3 & \frac{(\Delta x_3)^2}{4} & -\frac{(\Delta x_3)^3}{6} \end{bmatrix} \begin{bmatrix} y'_N \\ y''_N \\ y'''_N \end{bmatrix} \tag{3.32}$$

with $\Delta x_i = x_N - x_{N-i}$, $i = 1,2,3$.

Depending on the particular circumstances, approximations for $\frac{dx}{dy}$ at P_0 and P_N may be determined in a similar manner using Taylor expansions. The choice between determining $\frac{dy}{dx}$ or $\frac{dx}{dy}$ at P_0 and P_N depends on which of the following conditions are satisfied, and which are violated:

Condition 4(a):	$x_3 > x_2 > x_1 > x_0$
Condition 4(b):	$x_0 > x_1 > x_2 > x_3$
Condition 4(c):	$x_{N-3} > x_{N-2} > x_{N-1} > x_N$
Condition 4(d):	$x_N > x_{N-1} > x_{N-2} > x_{N-3}$
Condition 5(a):	$y_3 > y_2 > y_1 > y_0$
Condition 5(b):	$y_0 > y_1 > y_2 > y_3$
Condition 5(c):	$y_{N-3} > y_{N-2} > y_{N-1} > y_N$
Condition 5(d):	$y_N > y_{N-1} > y_{N-2} > y_{N-3}$

Table 3.5

Since four node points are involved in each condition, the clustered distributions of the nodal points P_0, P_1, P_2 and P_3, as well as P_5, P_6, P_7 and P_8 in Figure 3.7 are further justified considering the requirement that at least two of the conditions listed in Table 3.5 must be satisfied for any set of nodal points. In particular, at least *one* of conditions 4(a), 4(b), 5(a) or 5(b), and *one* of conditions 4(c), 4(d), 5(c) or 5(d) must be satisfied for the purposes of determining the sought after initial and final gradients.

For nodal points P_0, P_1, P_2 and P_3 shown in Figure 3.7 it is clear that both conditions 4(a) and 5(a) are satisfied, implying that either $\frac{dy}{dx}$ or $\frac{dx}{dy}$ can be determined at P_0. Similarly for nodal points P_5, P_6, P_7 and P_8, both conditions 4(c) and 5(c) are satisfied, implying that either $\frac{dy}{dx}$ or $\frac{dx}{dy}$ can be determined at $P_N = P_8$. In these eventualities, the appropriate choice is made by testing which of the additional conditions listed in Table 3.6 are satisfied.

Condition 6(a):	$\lvert x_3 - x_0 \rvert \geq \lvert y_3 - y_0 \rvert$
Condition 6(b):	$\lvert x_3 - x_0 \rvert < \lvert y_3 - y_0 \rvert$
Condition 7(a):	$\lvert x_N - x_{N-3} \rvert \geq \lvert y_N - y_{N-3} \rvert$
Condition 7(b):	$\lvert x_N - x_{N-3} \rvert < \lvert y_N - y_{N-3} \rvert$

Table 3.6

For example, since for nodes P_0 and P_3 shown in Figure 3.7, condition 6(a) is satisfied, the obvious choice is to determine $\frac{dy}{dx}$ at node P_0. Similarly, since condition 7(a) is satisfied for nodes P_5 and P_8, $\frac{dy}{dx}$ is to be determined at node $P_N = P_8$.

The following truth table shows how the conditions from Table 3.5 and Table 3.6 determine the form of the gradient to be used at node P_0. As before, the rows show different combinations of satisfied and violated conditions, where a 1 indicates that the specific condition is satisfied, and a 0 that it is violated.

Condition 4(a)	**Condition 4(b)**	**Condition 5(a)**	**Condition 5(b)**	**Condition 6(a)**	**Condition 6(b)**	**Gradient at P_0**
1	0	0	0			$\frac{dy}{dx}$
0	1	0	0			$\frac{dy}{dx}$
0	0	1	0			$\frac{dx}{dy}$
0	0	0	1			$\frac{dx}{dy}$

1	0	1	0	1	0	$\frac{dy}{dx}$
				0	1	$\frac{dx}{dy}$
1	0	0	1	1	0	$\frac{dy}{dx}$
				0	1	$\frac{dx}{dy}$
0	1	1	0	1	0	$\frac{dy}{dx}$
				0	1	$\frac{dx}{dy}$
0	1	0	1	1	0	$\frac{dy}{dx}$
				0	1	$\frac{dx}{dy}$

Table 3.7

A similar truth table may be drawn up showing how the different combinations of conditions determine the form of the gradient to be used at P_N.

Of course, with $\frac{dy}{dx}$ (or $\frac{dx}{dy}$) determined at nodes P_0 and P_N using the above strategy, $\frac{dx}{dy}$ (or $\frac{dy}{dx}$) at nodes P_0 and P_N is simply given by the reciprocal relationship:

$$\frac{dx(y_i)}{dy} = \left[\frac{dy(x_i)}{dx}\right]^{-1} \text{ or } \frac{dy(x_i)}{dy} = \left[\frac{dx(y_i)}{dx}\right]^{-1} \text{ for } i = 1, N$$

3.3 Synthesis of more general curves

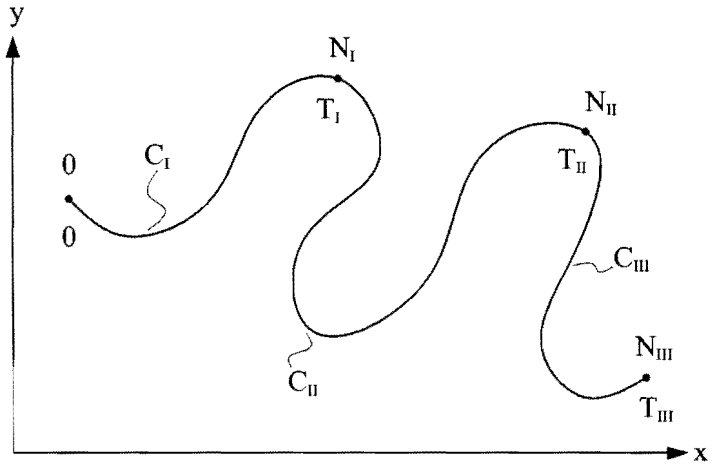

Figure 3.8: General curve where the prescribed speed is achieved.

Section 3.1.1.3 deals with the simplified situation of tangential acceleration along the prescribed curve until a specified tangential speed v^* is achieved at time $t_N = T$. A more realistic example is shown in Figure 3.8 where the motion is executed in three segments: tangential acceleration along curve C_I, constant tangential speed along curve C_{II}, and tangential deceleration along curve C_{III}. The set of nodal points associated with the general curve of Figure 3.8 is $\{P_i = (x_i, y_i), i = 0,1,...,N_I,...,N_{II},...,N_{III}\}$.

This Section proposes a methodology by means of which node numbers N_I and N_{II} may automatically be assigned, given the *prescribed* constant tangential speed v^* along C_{II} and the maximum *allowable* tangential acceleration $\ddot{s}_{ALLOW}$.

In what follows "speed" and "acceleration" refer to *tangential* speed and *tangential* acceleration, unless otherwise specified.

3.3.1 Linear segment with cubic blends

Assume that node numbers N_I and N_{II} are given. Node number N_{III} is automatically known, since it is the final node in the specified data series. Path lengths S_I, S_{II} and S_{III}, corresponding to the respective curves C_I, C_{II} and C_{III}, may then be determined by following the procedure outlined in Sections 3.1.1.1 and 3.1.1.2.

The acceleration curve C_I in Figure 3.8, corresponds to the situation already discussed in Section 3.1.1.3, i.e. a gradual increase in speed is required over the time interval $t \in [0, T_I]$, such that the prescribed speed v^* is attained at time T_I.

For curve C_I the distance along curve s_I at any instant t is represented by the cubic polynomial in time (see expression (3.15)):

$$s_I(t) = a_{sI} + b_{sI}\, t + c_{sI}\, t^2 + d_{sI}\, t^3,\ t \in [0, T_I] \tag{3.33}$$

$$\text{with quadratic expression } \dot{s}_I(t) = b_{sI} + 2c_{sI}\, t + 3d_{sI}\, t^2, \text{ for the speed} \tag{3.34}$$

$$\text{and linear form } \ddot{s}_I(t) = 2c_{sI} + 6d_{sI}\, t, \text{ for the acceleration} \tag{3.35}$$

The motion along the acceleration curve C_I is associated with boundary conditions that are similar to the ones given in Section 3.1.1.3; namely

$$s_I(0) = s_0 \text{ (usually } s_0 = 0)$$

$$s_I(T_I) = S_I$$

$$\dot{s}_I(0) = v_0 \text{ (usually } v_0 = 0)$$

$$\dot{s}_I(T_I) = v^*$$

$$\ddot{s}_I(T_I) = 0$$

The unknown coefficients a_{sI}, b_{sI}, c_{sI} and d_{sI}, as well as T_I are determined in exactly the same manner as explained in Section 3.1.1.1 (expressions (3.18) - (3.24)). With the coefficients and the time instant T_I known, the nodal times t_i, $i = 1,2,...,N_I$ may be obtained using Newton's method (see Section 3.1.1.3).

Along the constant speed segment C_{II} in Figure 3.8 the distance s_{II} along the curve from nodal point P_{N_I} is given by the following linear relationship in time:

$$s_{II}(t) = v^*(t - T_I),\ t \in [T_I, T_{II}] \tag{3.36}$$

For each node $P_i = (x_i, y_i)$, $i = N_I + 1, N_I + 2,..., N_{II}$, the total path length S_i from P_0 up to the specific node P_i may be determined from (3.25):

$$S_i = \sum_{j=1}^{i} s_j,\ i = N_I + 1, N_I + 2,..., N_{II} \tag{3.37}$$

The corresponding nodal times t_i, $i = N_I + 1, N_I + 2,..., N_{II}$ then follow from (3.36):

$$t_i = \frac{S_i - S_I}{v^*} + T_I,\ i = N_I + 1, N_I + 2,..., N_{II} \tag{3.38}$$

For the final deceleration segment C_{III} in Figure 3.8, the distance along the curve s_{III} from nodal point $P_{N_{II}}$ is also given by a cubic polynomial function of time:

$$s_{III}(t) = a_{sIII} + b_{sIII}(t - T_{II}) + c_{sIII}(t - T_{II})^2 + d_{sIII}(t - T_{II})^3,\ t \in [T_{II}, T_{III}] \tag{3.39}$$

$$\dot{s}_{III}(t) = b_{sIII} + 2c_{sIII}(t - T_{II}) + 3d_{sIII}(t - T_{II})^2 \tag{3.40}$$

$$\ddot{s}_{III}(t) = 2c_{sIII} + 6d_{sIII}(t - T_{II}) \tag{3.41}$$

Since a decrease in speed is required along the deceleration segment C_{III}, the following boundary conditions are enforced:

$$s_{III}(T_{II}) = S_{II}$$

$$s_{III}(T_{III}) = S_{III}$$

$$\dot{s}_{III}(T_{II}) = v^*$$

$$\dot{s}_{III}(T_{III}) = 0$$

$$\ddot{s}_{III}(T_{II}) = 0$$

from which the coefficients a_{sIII}, b_{sIII}, c_{sIII}, d_{sIII} and the final time instant T_{III} can be determined:

$$s_{III}(T_{II}) = a_{sIII} = S_{II}$$

$$\dot{s}_{III}(T_{II}) = b_{sIII} = v^*$$

$$\ddot{s}_{III}(T_{II}) = 2c_{sIII} = 0$$

$$\therefore c_{sIII} = 0$$

$$s_{III}(T_{III}) = S_{III} = a_{sIII} + b_{sIII}(T_{III} - T_{II}) + d_{sIII}(T_{III} - T_{II})^3 \tag{3.42}$$

$$\dot{s}_{III}(T_{III}) = 0 = b_{sIII} + 3d_{sIII}(T_{III} - T_{II})^2 \tag{3.43}$$

and with $b_{sIII} = v^*$ it follows from (3.43):

$$d_{sIII} = \frac{-v^*}{3(T_{III} - T_{II})^2} \tag{3.44}$$

and substituting (3.44) into (3.42):

$$T_{III} = \frac{3(S_{III} - S_{II})}{2v^*} + T_{II} \tag{3.45}$$

Newton's method is then used to determine the corresponding nodal times t_i, $i = N_{II} + 1, N_{II} + 2, \ldots, N_{III}$ in the manner already described in Section 3.1.1.3.

It follows that the motion, described in terms of the distance $s(t)$ along the general curve shown in Figure 3.8, is a *linear segment with cubic blends* (LSCB), since the cubic motions along curves C_I and

C_{III} are merged or blended with the constant velocity motion along curve C_{II} at the respective blend times T_I and T_{II} as shown in Figure 3.9 (see [60]).

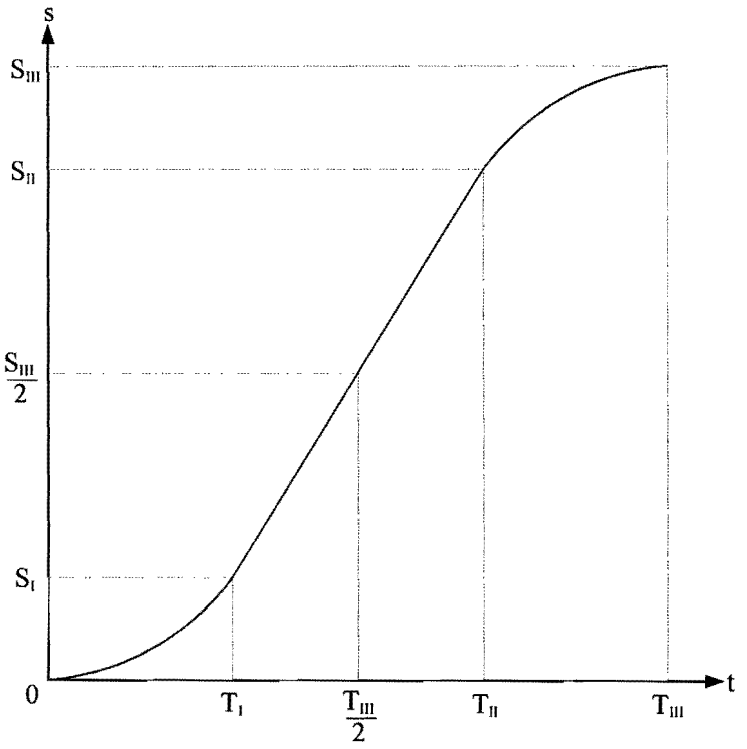

Figure 3.9: Linear segment with cubic blends (LSCB).

Blend time T_I is given by (3.24):

$$T_I = \frac{3(S_I - s_0)}{v_0 + 2v^*} \tag{3.46}$$

which reduces to $T_I = \frac{3S_I}{2v^*}$ with $s_0 = 0$ and $v_0 = 0$.

Similarly, blend time T_{II} is given by (3.45):

$$T_{III} - T_{II} = \frac{3(S_{III} - S_{II})}{2v^*} \tag{3.47}$$

The latter two equations indicate that if the nodal points N_I and N_{II} are chosen in such a way that $S_{III} - S_{II} = S_I$, then time spans $(T_I - 0)$ and $(T_{III} - T_{II})$ are equal. In this case the LSCB, as shown in Figure 3.9, is "centro-symmetric" with respect to the midpoint $\left[\frac{T_{III}}{2}, \frac{S_{III}}{2}\right]$ (see [60]).

Another important and desirable feature of the proposed LSCB motion, is the fact that the corresponding speed and acceleration curves are continuous as depicted in Figure 3.10.

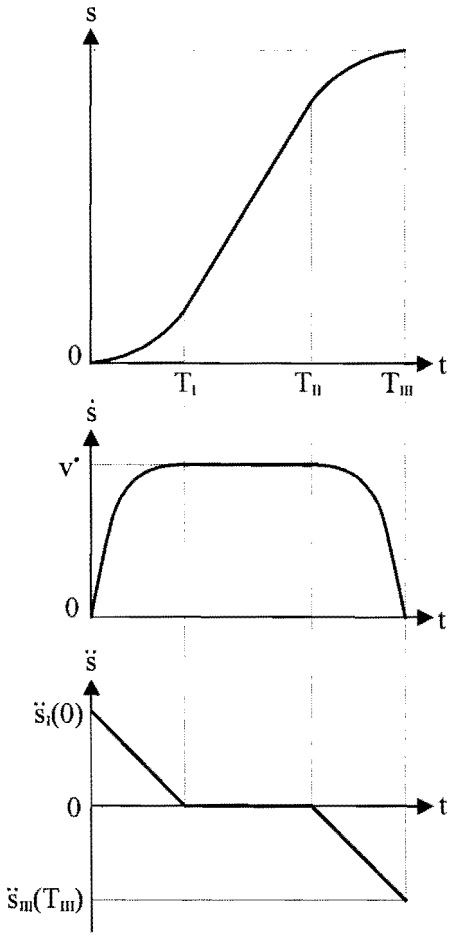

Figure 3.10: LSCB motion with its accompanying speed and acceleration curves.

The initial acceleration $\ddot{s}_I(0)$ is obtained by substituting (3.46) into (3.23) giving

$$c_{sI} = \frac{(v^* - v_0)(v_0 + 2v^*)}{3(S_I - s_0)}$$

which, after substituting into (3.35) yields

$$\ddot{s}(0)_I = 2c_{sI} = \frac{2(v^* - v_0)(v_0 + 2v^*)}{3(S_I - s_0)} \tag{3.48}$$

Expression (3.48) simplifies further if $v_0 = 0$ and $s_0 = 0$, as is usually the case, to give

$$\ddot{s}_I(0) = \frac{4(v^*)^2}{3S_I} \tag{3.49}$$

Further, by substituting $d_{sIII} = \frac{-v^*}{3(T_{III} - T_{II})^2}$ as well as (3.47) into (3.41), the final acceleration is given by

$$\ddot{s}_{III}(T_{III}) = \frac{-4(v^*)^2}{3(S_{III} - S_{II})} \tag{3.50}$$

If $S_{III} - S_{II} = S_I$, the magnitude of the initial acceleration $\ddot{s}_I(0)$ is equal to the magnitude of the final acceleration $\ddot{s}_{III}(T_{III})$ due to the symmetry that exists in this case (compare expressions (3.49) and (3.50)). It is of particular interest to note that for this symmetrical situation, the magnitudes of the accelerations at the initial and final times are not only equal but correspond to the *maximum* acceleration magnitude that occurs along the total curve.

3.3.2 Treatment of constraint on acceleration

The practical requirement that the prescribed motion is to be executed as fast as possible, is usually subject to a prescribed maximum *allowable* acceleration magnitude $\ddot{s}_{ALLOW}$. A procedure is now described that may be used to select appropriate node numbers N_I and N_{II} such that the following specific acceleration constraints are not violated:

$$\ddot{s}_I(0) \le \ddot{s}_{ALLOW} \tag{3.51}$$

$$\left|\ddot{s}_{III}(T_{III})\right| \le \ddot{s}_{ALLOW} \tag{3.52}$$

Since by (3.35) and (3.41) the acceleration along both C_I and C_{III} vary linearly with time, it follows that if the specific constraints (3.51) and (3.52) are satisfied, that the constraint on the acceleration is also satisfied at each instant along the whole path.

As before, for each node $P_i = (x_i, y_i)$, $i = 0,1,...,N_{III}$, the total path length up to the specific node may be determined using expression (3.25). A special nodal point N_{MID}, corresponding to a point approximately halfway along the total curve (i.e. for which $S_{N_{MID}} \approx \frac{S_{III}}{2}$) can be identified using the following criterion:

$$S_{MID} \le \frac{S_{III}}{2} < S_{MID+1} \tag{3.53}$$

As a first iteration in finding the appropriate choices for nodes N_I and N_{II}, assume that nodes N_I and N_{II} coincide with node N_{MID} as shown in Figure 3.11.

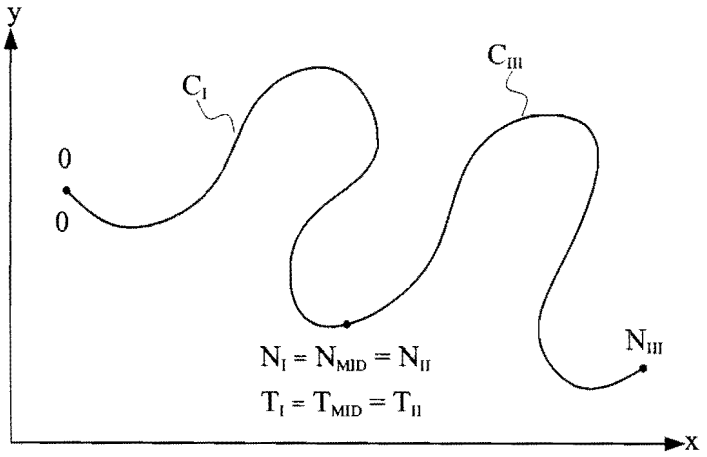

Figure 3.11: General curve showing the midpoint N_{MID}.

From (3.53) it follows that $S_{III} - S_{MID} \geq S_{MID}$, and with nodes N_I and N_{II} coinciding with node N_{MID}, it further follows that $S_{III} - S_{II} \geq S_I$ which, when substituted into (3.49) and (3.50), gives

$$\left|\ddot{s}_{III}(T_{III})\right| \leq \ddot{s}_I(0) \qquad (3.54)$$

Consequently, for the situation depicted in Figure 3.11, if the initial acceleration $\ddot{s}_I(0)$ satisfies constraint (3.51), the final acceleration $\ddot{s}_{III}(T_{III})$ will also satisfy constraint (3.52) and, indeed, the constraint on the magnitude of the acceleration will be satisfied at each instant along the total curve.

3.3.2.1 Attainment of central speed v^*

If the initial acceleration for the situation shown in Figure 3.11 satisfies constraint (3.51), the desired central speed v^* may be reached at node N_{MID}. For practical purposes the ideal objectives are, however:

1. to attain the desired central speed v^* in the *shortest* possible time T_I without exceeding the allowable maximum acceleration magnitude $\ddot{s}_{ALLOW}$, and
2. to maintain the desired speed v^* for the *longest* possible time span $(T_{II} - T_I)$ provided that, over the final time interval $[T_{II}, T_{III}]$, the maximum deceleration magnitude does not exceed the allowable magnitude $\ddot{s}_{ALLOW}$.

With reference to objective 1 above, expressions (3.46) and (3.48) respectively indicate that for a specific speed v^*, a shorter path length S_I will result in a shorter time T_I and a larger initial acceleration $\ddot{s}_I(0)$. By shifting, for example, node N_I to coincide with node $N_{MID} - 1$ the associated path length S_I and corresponding time T_I will be reduced, while the associated initial acceleration $\ddot{s}_I(0)$ will become larger. This increased initial acceleration is then tested against constraint (3.51), and if the constraint is

still satisfied, node N_I is shifted further to coincide with node $N_{MID}-2$. These integer shifts are continued until, after p integer shifts, the choice of node N_I, coinciding with node $N_{MID}-p$, is such that the initial acceleration satisfies constraint (3.51), while the choice $N_I = N_{MID}-(p+1)$ violates the constraint.

With regard to objective 2, inspection of expressions (3.47) and (3.50), indicates that a decrease in the path length $(S_{III}-S_{II})$ will result in a shorter time span $(T_{III}-T_{II})$, and a larger final acceleration magnitude $|\ddot{s}_{III}(T_{III})|$. For example, if node N_{II} is shifted to coincide with node $N_{MID}+1$ and thus shortens the path length $(S_{III}-S_{II})$ and the time span $(T_{III}-T_{II})$, it will result in a larger final acceleration magnitude $|\ddot{s}_{III}(T_{III})|$. If the larger $|\ddot{s}_{III}(T_{III})|$ satisfies constraint (3.52), node N_{II} may be shifted further to coincide with node $N_{MID}+2$, etc. These integer shifts may be continued until, after q shifts, node N_{II}, coinciding with node $N_{MID}+q$ is such that the final acceleration magnitude $|\ddot{s}_{III}(T_{III})|$ satisfies constraint (3.52), while the choice $N_{II} = N_{MID}+(q+1)$ violates the constraint.

3.3.2.2 Violation of maximum allowable acceleration

If the initial acceleration, for the situation depicted in Figure 3.11 with specified central velocity v^*, violates constraint (3.51), a different strategy is proposed which ensures that the maximum allowable acceleration is not exceeded. For this case, the motion along the curve shown in Figure 3.11, consists of two blended cubic polynomials in time. The blend time is T_{MID} as shown in Figure 3.12:

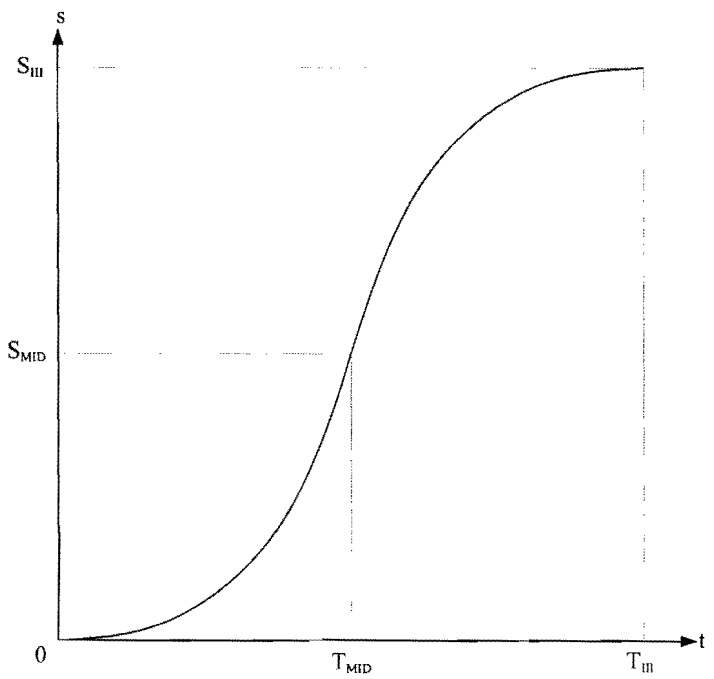

Figure 3.12: Blended cubic polynomials.

More specifically, the two objectives set in this case are:

1. to accelerate as fast as possible along curve C_I without violating constraint (3.51), and
2. to decelerate as fast as possible along curve C_{II} without violating constraint (3.52).

Objective 1 implies a different set of boundary conditions for determining the coefficients of the cubic polynomial function representing the path length along curve C_I (see expression (3.33)). These new boundary conditions are

$$s_I(0) = s_0 \text{ (usually } s_0 = 0)$$

$$s_I(T_{MID}) = S_{MID}$$

$$\dot{s}_I(0) = v_0 \text{ (usually } v_0 = 0)$$

$$\ddot{s}_I(0) = \ddot{s}_{ALLOW}$$

$$\ddot{s}_I(T_{MID}) = 0$$

from which a_{sI}, b_{sI}, c_{sI}, d_{sI}, and T_{MID} may be determined as follow:

$$s_I(0) = a_s = s_0$$

$$\dot{s}_I(0) = b_s = v_0$$

$$\ddot{s}_I(0) = \ddot{s}_{ALLOW} = 2c_{sI}$$

$$\text{and therefore } c_{sI} = \frac{\ddot{s}_{ALLOW}}{2},$$

$$s_I(T_{MID}) = S_{MID} = a_{sI} + b_{sI} T_{MID} + c_{sI}(T_{MID})^2 + d_{sI}(T_{MID})^3 \tag{3.55}$$

$$\ddot{s}_I(T_{MID}) = 0 = 2c_{sI} + 6d_{sI} T_{MID} \tag{3.56}$$

and thus

$$d_{sI} = \frac{-\ddot{s}_{ALLOW}}{6T_{MID}} \tag{3.57}$$

Substituting (3.57) into (3.55): $s_I(T_{MID}) = S_{MID} = s_0 + v_0 T_{MID} + \frac{\ddot{s}_{ALLOW}}{3}(T_{MID})^2$

$$\text{which gives } T_{MID} = \frac{-v_0 \pm \sqrt{v_0^2 - 4\left(\frac{\ddot{s}_{ALLOW}}{3}\right)(s_0 - S_{MID})}}{2\left(\frac{\ddot{s}_{ALLOW}}{3}\right)}$$

and which reduces to

$$T_{MID} = \pm\sqrt{\frac{3S_{MID}}{\ddot{s}_{ALLOW}}} \tag{3.58}$$

if $s_0 = 0$ and $v_0 = 0$

The positive root gives the sought after time instant T_{MID}.

From (3.34) and substituting the values of the coefficients determined above, the speed at node N_{MID} is

$$v_{MID} = \dot{s}_I(T_{MID}) = v_0 + \frac{\ddot{s}_{ALLOW}}{2} T_{MID}$$

which reduces to

$$v_{MID} = \dot{s}_I(T_{MID}) = \frac{\sqrt{3S_{MID}\ddot{s}_{ALLOW}}}{2} \qquad (3.59)$$

if $s_0 = 0$ and $v_0 = 0$.

The cubic polynomial function of time representing the deceleration segment C_{III} in Figure 3.11 is given by expression (3.39). The unknown coefficients a_{sIII}, b_{sIII}, c_{sIII} and d_{sIII} as well as T_{III} are solved for by using similar boundary conditions as before:

$$s_{III}(T_{II}) = S_{MID}$$

$$s_{III}(T_{III}) = S_{III}$$

$$\dot{s}_{III}(T_{II}) = v_{MID}$$

$$\dot{s}_{III}(T_{III}) = 0$$

$$\ddot{s}_{III}(T_{II}) = 0$$

Substituting these conditions in the corresponding general expressions (3.39), (3.40) and (3.41) for s, $\dot{s}$ and $\ddot{s}$, and following the identical steps represented by equations (3.42) to (3.45) finally yields:

$$a_{sIII} = S_{MID}$$

$$b_{sIII} = v_{MID}$$

$$c_{sIII} = 0$$

$$d_{sIII} = \frac{-v_{MID}}{3(T_{III} - T_{MID})^2}$$

$$\text{and } T_{III} = \frac{3(S_{III} - S_{MID})}{2v_{MID}} + T_{MID}$$

As with the LSCB motion (see Figure 3.10), the blended cubic polynomials also result in continuous speed and acceleration curves as shown in Figure 3.13.

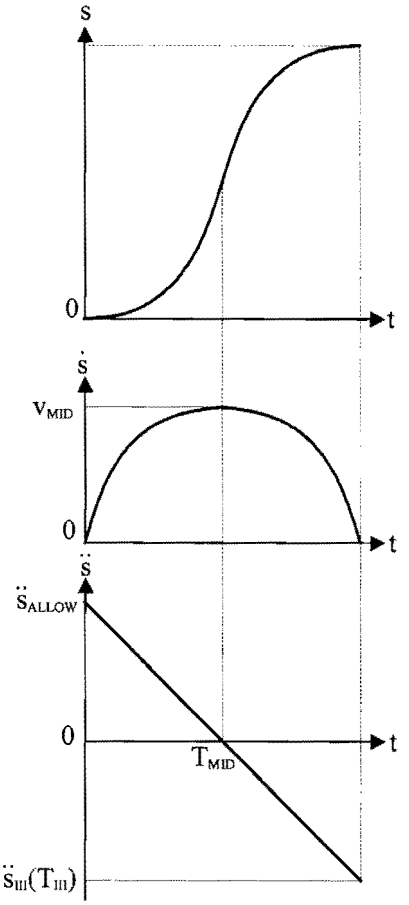

Figure 3.13: Blended cubic polynomials motion with its associated speed and acceleration curves.

From the above acceleration curve, it is clear that the initial acceleration is equal to the allowable maximum acceleration, i.e. $\ddot{s}_I(0) = \ddot{s}_{ALLOW}$. Since the final acceleration magnitude $|\ddot{s}_{III}(T_{III})|$ is either smaller than or equal to the initial acceleration magnitude $\ddot{s}_I(0)$ (see expression (3.54)), $|\ddot{s}_{III}(T_{III})|$ automatically satisfies acceleration constraint (3.52).

3.4 Incorporation of an orientation angle ϕ.

For certain applications of planar motion, the time parametric curves X(t) and Y(t) that interpolate the given set of nodal points $\{P_i = (x_i, y_i), i = 0,1,...,N\}$, are insufficient for the control of the particular mechanism, e.g. for a planar mechanism where the end-effector is to be orientated in a prescribed manner with respect to the tangent of the given path.

As an example, consider the situation where the orientation of the end-effector is to be exactly tangential to the curve, as the working point on the end-effector progresses along the prescribed curve. The gradient angle θ at any point along the curve is given by

$$\tan\theta = \frac{dy}{dx} \approx \frac{dp_i(x)}{dx} \text{ or } \left[\frac{dp_i(y)}{dy}\right]^{-1} \tag{3.60}$$

Another convenient form of expression (3.60) is

$$\tan\theta = \frac{\left(\frac{dy}{dt}\right)}{\left(\frac{dx}{dt}\right)} \approx \frac{\dot{Y}(t)}{\dot{X}(t)} \tag{3.61}$$

With the time parametric curves $X(t)$ and $Y(t)$ known, the respective derivatives $\dot{X}(t)$ and $\dot{Y}(t)$ are also known. Expression (3.61) may therefore be evaluated at nodal points P_i, $i = 0,1,...,N$ to find the corresponding values of θ_i, $i = 0,1,...,N$. As will be described below, the actual orientation angle ϕ of the end-effector is related to the angle θ in a non-straightforward manner as the working point executes the path.

In computing θ, care must be taken at nodes P_0 and P_N, since the respective speeds at these nodes are often zero, i.e. $\dot{s}_I(0) = v_0 = 0$ and $\dot{s}_{III}(T_{III}) = 0$. With this being the case, $\dot{X}(0) = \dot{Y}(0) = 0$ and $\dot{X}(T_{III}) = \dot{Y}(T_{III}) = 0$, and consequently expression (3.60) must be used instead of (3.61) to determine θ_0 and θ_N, since $\frac{dy}{dx}$ is known at nodes P_0 and P_N (see Section 3.2).

Since the arc tan function, through which θ is determined via (3.60) or (3.61), only assumes values between $-90°$ and $+90°$, a special procedure must be adopted to determine the exact orientation angle ϕ as the working point on the orientated end-effector tangentially follows the prescribed curve.

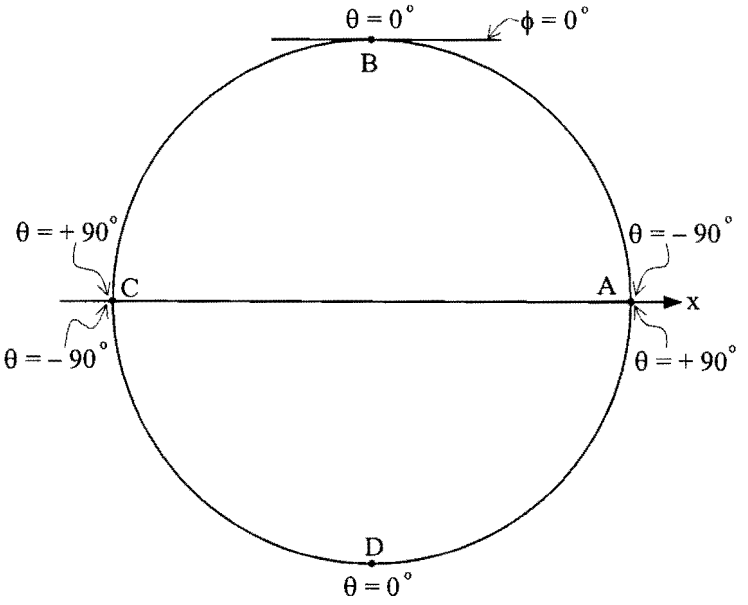

Figure 3.14: Circular prescribed curve.

Consider, for example, a prescribed circular curve as shown in Figure 3.14 with zero *orientation angle* ϕ at B. Starting at point A with θ and $\phi = -90°$ and progressing counterclockwise (CCW) around the circular curve the *gradient angle* θ computed via (3.60) or (3.61) gradually increases with ϕ from $-90°$ at A, to $0°$ at B, to $+90°$ at C. The CCW crossing of the x-axis at point C is however associated with a jump of $-180°$ in the computed *gradient angle* θ although ϕ is still clearly increasing continuously. Progressing CCW along the lower half of the circle again sees a gradual increase in the *gradient angle* θ from $-90°$ at C, to $0°$ at D, to $+90°$ at A, while ϕ continues to increase from $90°$ to $270°$ at A. At A where another jump of $-180°$ occurs in the computed value θ if the X-axis is crossed CCW.

A similar pattern is recognized using a clockwise (CW) tracing of the circular curve. Starting at point A, the computed *gradient angle* θ gradually decreases from $+90°$ at A, to $0°$ at D, to $-90°$ at C while ϕ decreases from $-90°$ at A to $-270°$ at C. The $+180°$ jump that occurs in θ with the CW crossing of the x-axis at C is followed by another gradual decrease in the *gradient angle* starting from $+90°$ at C, to $0°$ at B, to $-90°$ at A, while clearly ϕ continues to decrease from $-270°$ at C to $-450°$ at A.

The above-explained behavior of the *gradient angle* θ is used in establishing a procedure to determine the *orientation angle* ϕ:

If the jump between any two successive *gradient angles* θ_{i-1} and θ_i, $i = 1,2,...,N$ is smaller than $-90°$, i.e. $\theta_i - \theta_{i-1} \leq -90°$, a CCW-counter I_{CCW} is incremented. Further reflection indicates that I_{CCW} should

also be incremented if $0 < \theta_i - \theta_{i-1} < 90°$. Similarly if $\theta_i - \theta_{i-1} \geq 90°$ or $-90° < \theta_i - \theta_{i-1} < 0$, a CW-counter I_{CW} is incremented. Using these counters, the true associated *orientation angles* ϕ_i, $i = 1,2,...,N$ are given by

$$\phi_i = \theta_i + (I_{CCW})(180°) \tag{3.62}$$

if $0 < \theta_i - \theta_{i-1} < 90°$, or $\theta_i - \theta_{i-1} \leq -90°$, and

$$\phi_i = \theta_i - (I_{CW})(180°) \tag{3.63}$$

if $-90° < \theta_i - \theta_{i-1} < 0$, or $\theta_i - \theta_{i-1} \geq 90°$

In general expressions (3.62) and (3.63) respectively are given by:

$$\phi_i = \theta_i + (I_{CCW})(180°) + \phi_{offset} \tag{3.64}$$

if $0 < \theta_i - \theta_{i-1} < 90°$, or $\theta_i - \theta_{i-1} \leq -90°$, and

$$\phi_i = \theta_i - (I_{CW})(180°) + \phi_{offset} \tag{3.65}$$

if $-90° < \theta_i - \theta_{i-1} < 0$, or $\theta_i - \theta_{i-1} \geq 90°$

The term ϕ_{offset} in expressions (3.64) and (3.65) is defined as the *offset orientation angle* of the end-effector measured in a CCW convention from the tangent to the prescribed path at the point of contact as shown in Figure 3.15.

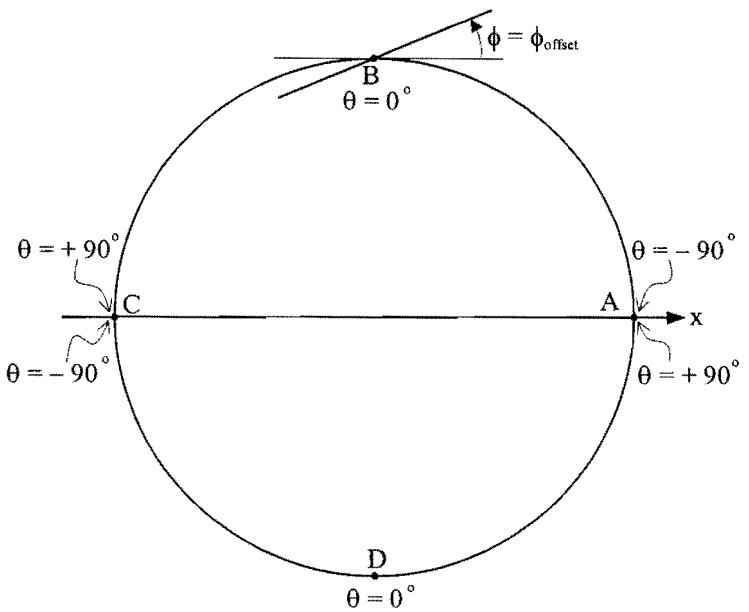

Figure 3.15: Circular prescribed curve with an angular offset added to the end-effector orientation.

Since the time instants t_i, $i = 0,1,2,...,N$ are known (see Section 3.1.1.3), a cubic spline representation $\Phi(t)$ may now be determined in exactly the same way as the cubic spline representations $X(t)$ and

$Y(t)$ (see Section 3.1.2). With the cubic spline $\Phi(t)$ known, the *continuous* first and second derivatives $\dot{\Phi}(t)$ and $\ddot{\Phi}(t)$ follow automatically.

Any prescribed path may also be traced with the end-effector posed in a specified fixed orientation ϕ_{fix}, thus eliminating the need to determine the cubic spline $\Phi(t)$ with its first and second derivatives $\dot{\Phi}(t)$ and $\ddot{\Phi}(t)$.

3.5 Test problems

The proposed trajectory planning methodology using **O**verlapping **C**ubic **A**rcs and (cubic) **S**plines (OCAS) is tested here on five different test functions. **Appendix B** contains a flow chart of the OCAS trajectory planning methodology.

3.5.1 Parabolic test function

The first test function is a parabola, where y is the quadratic function of x:

$$y(x) = \frac{x^2}{2} \tag{3.66}$$

The accuracy of the approximating fit is dependent on the number and distribution of the given nodal points $\{P_i = (x_i, y_i), i = 0,1,...,N\}$. The parabolic test function is approximated over the x-interval $x \in [-2,2]$ using 29 points spaced in such a way that they are more densely distributed at the beginning and end of the interval (see Figure 3.16). This is done to increase the accuracy of the calculation of the initial gradient $\frac{dy}{dx}$ at P_0 and final gradient $\frac{dy}{dx}$ at P_N as explained in Section 3.2. The nodal points are, for the obvious reason of greater accuracy, chosen more densely in neighborhood of the turning point where the greatest change in direction occurs.

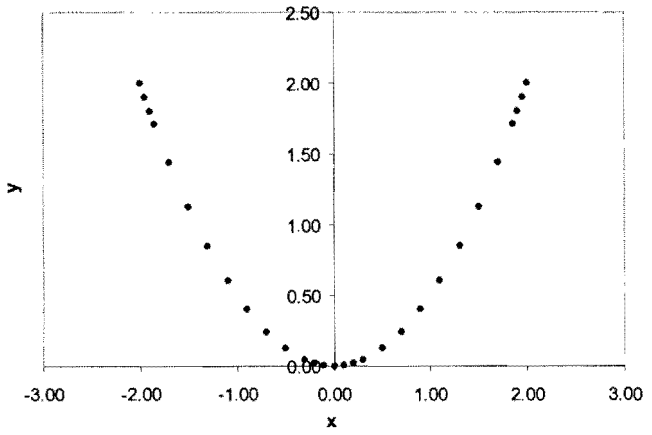

Figure 3.16: Nodal points used to approximate the parabolic test function.

In order to determine its accuracy, the fitted approximation is evaluated at chosen intermediate points between the pairs of consecutive nodes shown in Figure 3.16. Since the proposed OCAS-approach results in cubic spline representations for $X(t)$ and $Y(t)$ (see Section 3.1.2) over the time span between each pair of consecutive nodes, i.e. over $t_i - t_{i-1}$, $i = 1,2,...,28$, each interval may be subdivided to obtain a specified number of equally spaced additional *intermediate* time instants. The respective cubic spline representations $X(t)$ and $Y(t)$ are then evaluated at the *intermediate* time instants to give the corresponding *approximated intermediate* x- and y-values along the curve. Each approximated intermediate x-value lies in the interval $x \in [-2,2]$, and may therefore be substituted into (3.66) to find the corresponding *actual* y-value. For each intermediate x-value, the y-error is taken as the *absolute difference* between the *approximated* y-value and the *actual* y-value.

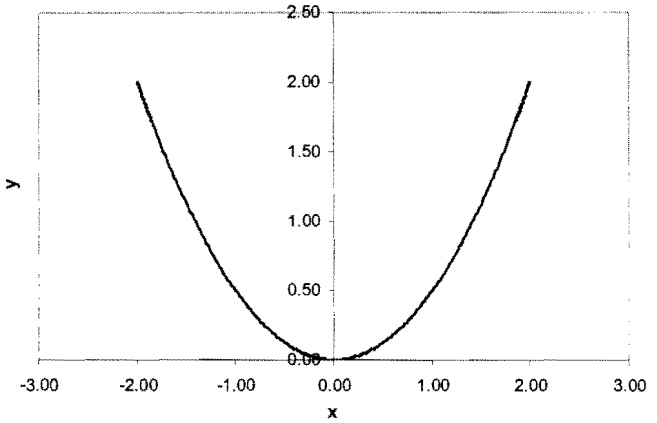

Figure 3.17: OCAS-approximation of parabolic test function.

Figure 3.17 shows the x-y profile obtained from the OCAS-approximation. Each consecutive time span $t_i - t_{i-1}$, $i = 1,2,...,28$ is divided into 10 equal subintervals and the curve in Figure 3.17 therefore represent a plot at 281 division points. The maximum absolute y-error over this set of points is 4.470×10^{-5} with an average error of 5.222×10^{-6}.

The trajectory planning along the parabolic profile was done by specifying a maximum allowable acceleration magnitude of 0.7 meter per second square, i.e. $\ddot{s}_{ALLOW} = 0.7$, and a specified central speed of 1.0 meter per second, i.e. $v^* = 1.0$. These specifications resulted in the LSCB-motion (see Section 3.3.1) shown in Figure 3.18. The blend times are $T_I = 2.922\,s$ and $T_{II} = 4.942\,s$ with the final time $T_{III} = 7.864\,s$. The initial acceleration is $\ddot{s}_I(0) = 0.684$ and the final acceleration is $\ddot{s}_{III}(T_{III}) = -0.684$ the magnitudes of which are both less than the specified maximum allowable acceleration magnitude $\ddot{s}_{ALLOW} = 0.7$.

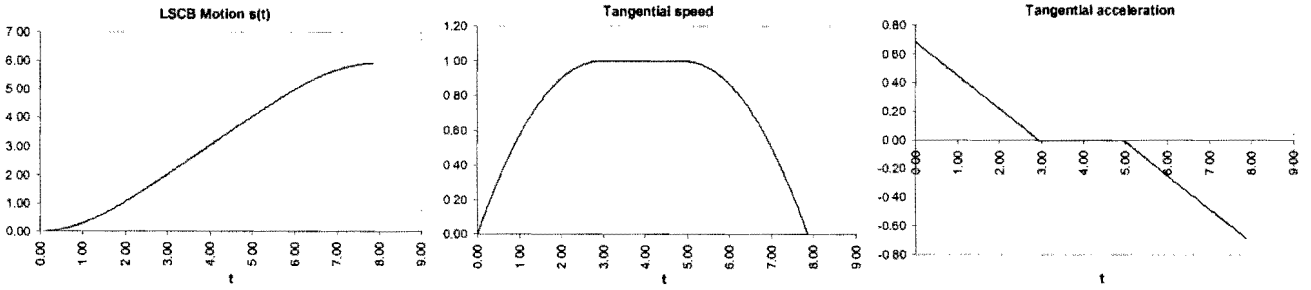

Figure 3.18: LSCB-motion for parabolic test function with its associated speed and acceleration curves.

The cubic spline representations $X(t)$ and $Y(t)$ that represent the x- and y-coordinate positions as functions of time, and plotted at the 281 time instants, are shown in Figure 3.19, together with the graphs of the continuous x- and y- velocities ($\dot{X}(t)$ and $\dot{Y}(t)$ designated as Vx and Vy) and accelerations ($\ddot{X}(t)$ and $\ddot{Y}(t)$ designated as Ax and Ay) over the total time interval $[0, 7.864]$. Note that the start point and end point of the prescribed trajectory follows from the cubic spline representations $X(t)$ and $Y(t)$, i.e. $(-2, 2)$ at $t = 0$ and $(2, 2)$ at $t = 7.864\,s$.

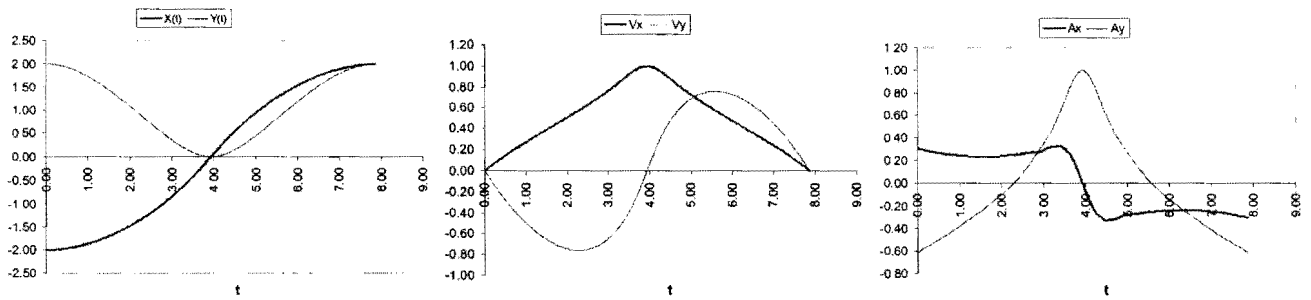

Figure 3.19: Plots of approximate coordinate positions, –velocities and –accelerations versus time for the parabolic test function.

With the specification that the end-effector be tangentially orientated with respect to the prescribed curve, (see Section 3.4), the cubic spline approximation $\Phi(t)$ representing the orientation angle ϕ [degrees] over the time interval $[0, 7.864]$ may be determined and is shown in Figure 3.20. Also shown in Figure 3.20 are the continuous orientation angular velocity curve $\dot{\Phi}(t)$ [rad/s] as well as the continuous orientation angular acceleration curve $\ddot{\Phi}(t)$ [rad/s^2].

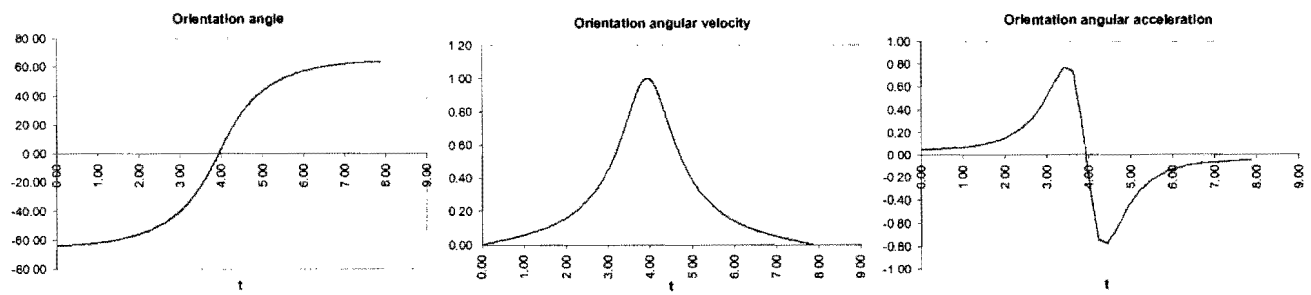

Figure 3.20: Plots of approximate orientation angle, orientation angular velocity and -acceleration for the parabolic test function.

3.5.2 *Spike test function*

The second test function is a spike test function taken from [68]:

$$y(x) = \frac{1}{1+x^2} \tag{3.67}$$

This spike test function is also approximated over the x-interval $x \in [-2,2]$. The initial and final nodal points are $P_0 = (x_0, y_0) = (2, 0.2)$ and $P_N = (x_N, y_N) = (-2, 0.2)$ respectively. In total 27 nodal points are specified as shown in Figure 3.21, with denser distributions of nodal points at the end points of the interval, as well as at the midpoint as is evident in Figure 3.21.

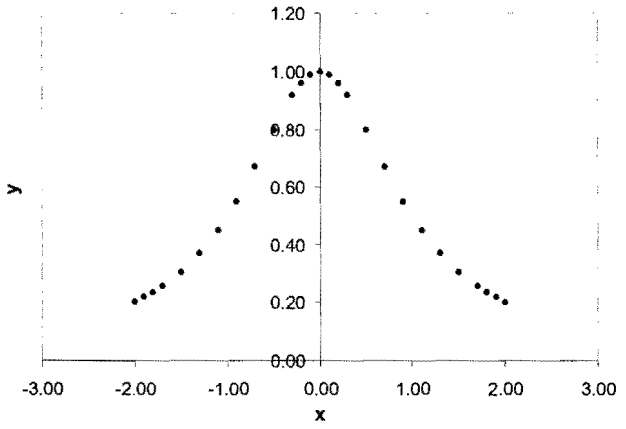

Figure 3.21: Nodal points used to specify the spike test function.

As in the case of the parabolic test function of Section 3.5.1, each consecutive time span $t_i - t_{i-1}$, $i = 1,2,...,26$ is divided into 10 subintervals by equally spaced additional time instants. The approximate x-y profile is drawn by plotting the values at the 261 division points as shown in Figure 3.22. Here the absolute maximum y-error resulting from this approximation is 1.359×10^{-4} with average error 1.201×10^{-5}.

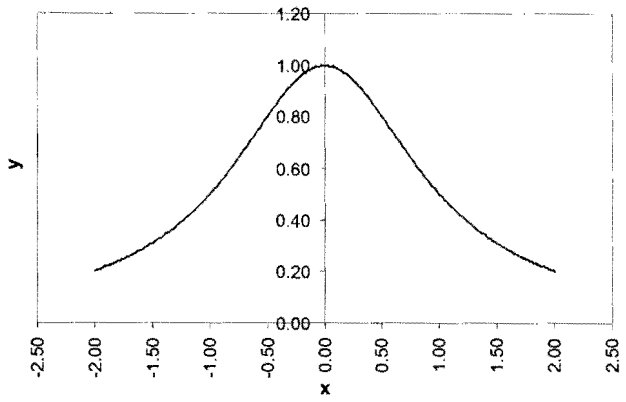

Figure 3.22: OCAS-approximation of spike test function.

With a specified central speed of $v^* = 1.0$ meter per second, and a specified maximum allowable acceleration $\ddot{s}_{ALLOW} = 0.5\,m/s^2$, the resulting motion is described by two blended cubic polynomials (see Section 3.3.2.2), as shown in Figure 3.23. The associated blend time is $T_{MID} = 3.6148\,s$, and from the tangential speeds graph in Figure 3.23 it is clear that the speed at the blend time, $v_{MID} = 0.9037\,m/s$, is slightly less that the desired speed of $v^* = 1.0\,m/s$. This is due to the fact that the magnitudes of both the initial and final curvature accelerations are equal to the maximum allowable acceleration of $\ddot{s}_{ALLOW} = 0.5\,m/s^2$.

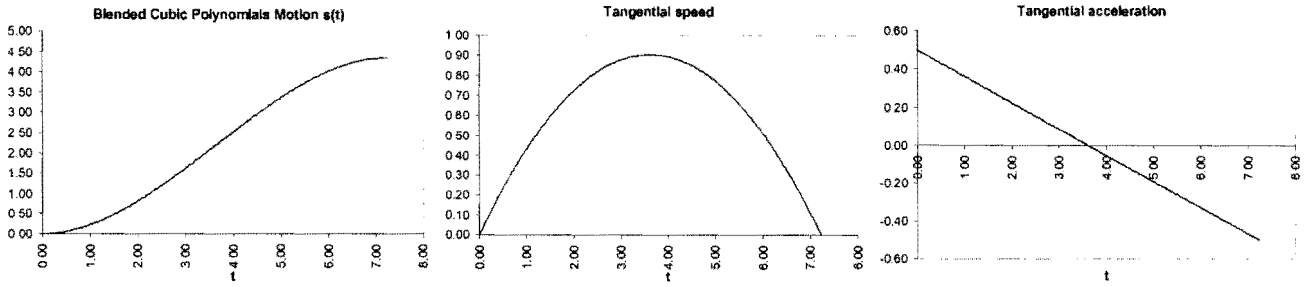

Figure 3.23: Blended cubic polynomials motion for spike test function with its associated speed and acceleration curves.

Figure 3.24 shows plots of the x- and y-positions $X(t)$ and $Y(t)$ (with start point $(2, 0.2)$ at $t = 0$ and end point $(-2, 0.2)$ at $t = 7.230\,s$), the x- and y-velocities $\dot{X}(t)$ and $\dot{Y}(t)$ (designated as Vx and Vy), and the x- and y-accelerations $\ddot{X}(t)$ and $\ddot{Y}(t)$ (designated as Ax and Ay) at the 261 time instants distributed over the time interval $[0, 7.230]$.

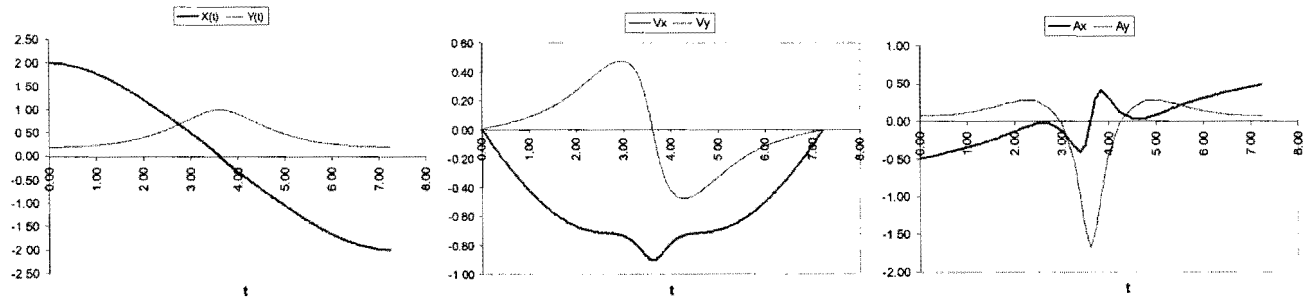

Figure 3.24: Plots of the approximate coordinates, velocities and accelerations versus time for the spike test function.

The tangentially orientated end-effector specification results in the cubic spline approximation $\Phi(t)$ [degrees] plotted in Figure 3.25, together with the corresponding plots of the continuous orientation angular velocity curve $\dot{\Phi}(t)$ [rad/s], and the continuous orientation angular acceleration curve $\ddot{\Phi}(t)$ [rad/s^2].

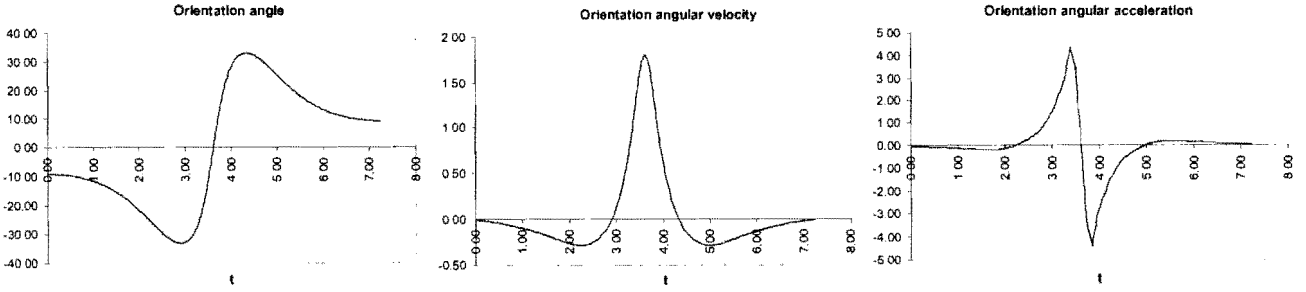

Figure 3.25: Plots of approximate orientation angle, orientation angular velocity and acceleration versus time for the spike test function.

In order to verify expressions (3.64) and (3.65), an orientation angle offset $\phi_{offset} = 30^{\circ}$ is specified, and the associated cubic spline approximation $\Phi(t)$ [degrees] is plotted in Figure 3.26. Also shown in Figure 3.26 are the corresponding plots of the continuous orientation angular velocity curve $\dot{\Phi}(t)$ $[\text{rad}/\text{s}]$, and the continuous angular acceleration curve $\ddot{\Phi}(t)$ $[\text{rad}/\text{s}^2]$.

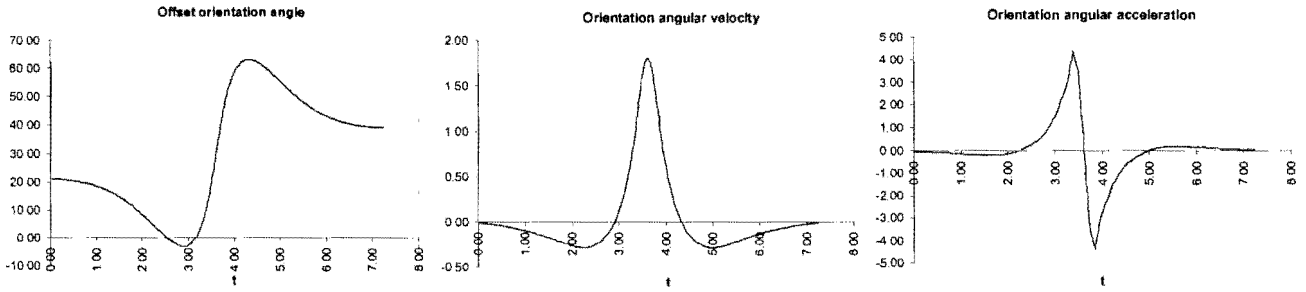

Figure 3.26: Plots of approximate offset orientation angle, orientation angular velocity and acceleration versus time for the spike test function.

Comparing the *offset* cubic spline approximation $\Phi(t)$ of Figure 3.26 with the *tangential* cubic spline approximation $\Phi(t)$ of Figure 3.25, it is clear that the specified offset ($\phi_{offset} = 30^{\circ}$) resulted in an *upward* shift of the orientation angle curve. As expected, the orientation angular velocity and orientation angular acceleration curves of Figures 3.25 and 3.26 are in exact agreement.

3.5.3 Circular test curve

The ability of the proposed OCAS-approach to approximate curves that cannot be represented by unique-valued functions of one coordinate variable in terms of the other, is demonstrated here for the circle:

$$x^2 + y^2 = 9 \tag{3.68}$$

The nodal points $\{P_i = (x_i, y_i), i = 0,1,...,N\}$ are specified using corresponding sweep angles $\beta_i \in [0^{\circ}, 720^{\circ}]$, where the sweep angle is measured clockwise from the positive x-axis. For any specific

sweep angle β_i, $i = 0,1,...,N$ the corresponding x- and y-values are given by $x_i = 3\cos\beta_i$, and $y_i = 3\sin\beta_i$ respectively. Here the sequence of sweep angles $\{\beta_i\}$ is chosen such that starting at $\beta = 0°$, two complete CCW revolutions are followed.

The spacing of the nodal points is again clustered around the beginning and end of the total interval as can be seen in Figure 3.27. A total of 79 nodal points cover the two revolutions of the circular path. The nodes for each revolution are shown separately in Figure 3.27. In particular, the first revolution ($\beta \in [0, 360°]$) is shown on the left-hand side of Figure 3.27, and the second revolution ($\beta \in [360°, 720°]$) is shown on the right-hand side of Figure 3.27.

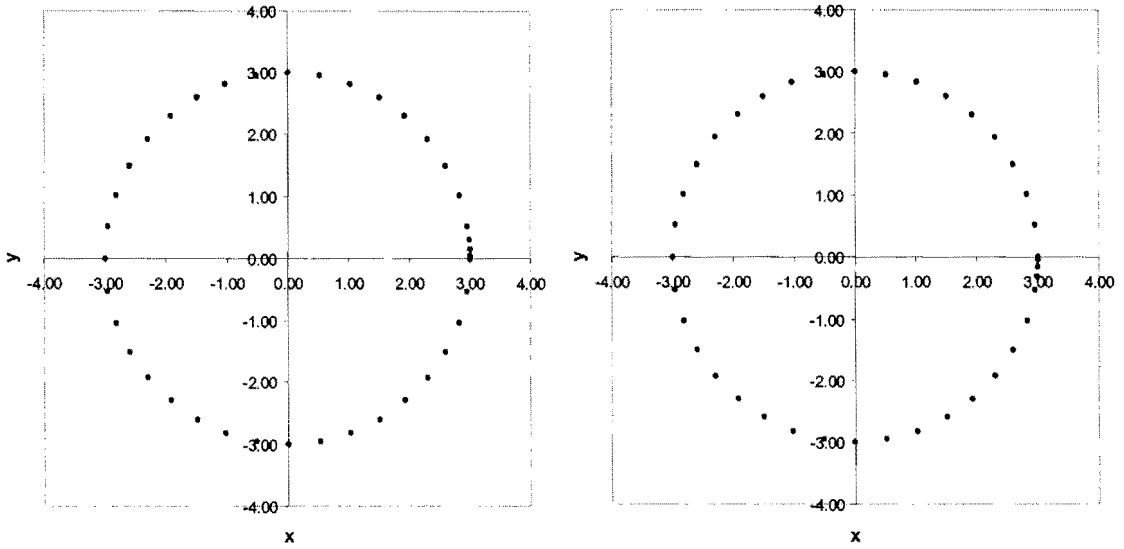

Figure 3.27: Nodal points used to approximate two revolutions of the circular curve.

As before, each time span $t_i - t_{i-1}$, $i = 1,2,...,78$ is divided into 10 equal subintervals for the purpose of mapping the computed approximation at the division points (see Section 3.5.1). The x-y-profile obtained from the OCAS-approximation at the specified division points is shown in Figure 3.28. For any given time instant the approximated x- and y-coordinates correspond to an *approximated* radius, from which the absolute radius error can be calculated. The maximum absolute radius error computed over the 781 division points is 5.27×10^{-5} with an average error of 6.27×10^{-6}.

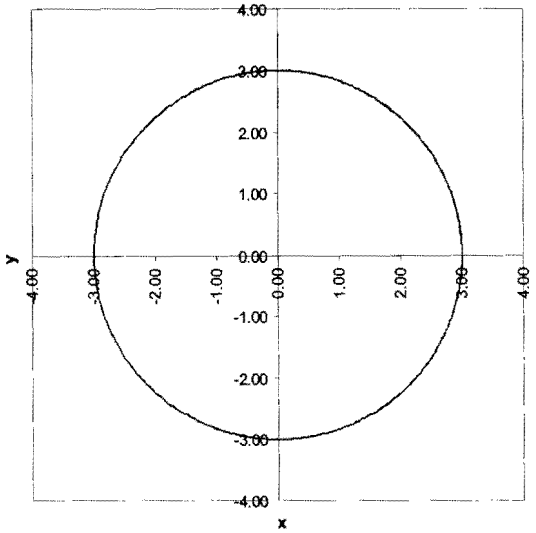

Figure 3.28: OCAS-approximation of circular test curve.

The trajectory planning is done by limiting the maximum allowable acceleration to 0.5 meter per second square, i.e. $\ddot{s}_{ALLOW} = 0.5\,m/s^2$, and by specifying a central speed of 1.0 meter per second, i.e. $v^* = 1.0\,m/s$. These specifications resulted in a LSCB- motion with corresponding blend times $T_I = 4.712\,s$ and $T_{II} = 36.127\,s$ (see Figure 3.29) and total path time $T_{III} = 40.841\,s$. The initial and final tangential accelerations are $\ddot{s}_I(0) = 0.424\,m/s^2$ and $\ddot{s}_{III}(T_{III}) = -0.424\,m/s^2$ both satisfying the bound on the magnitude of accelerations.

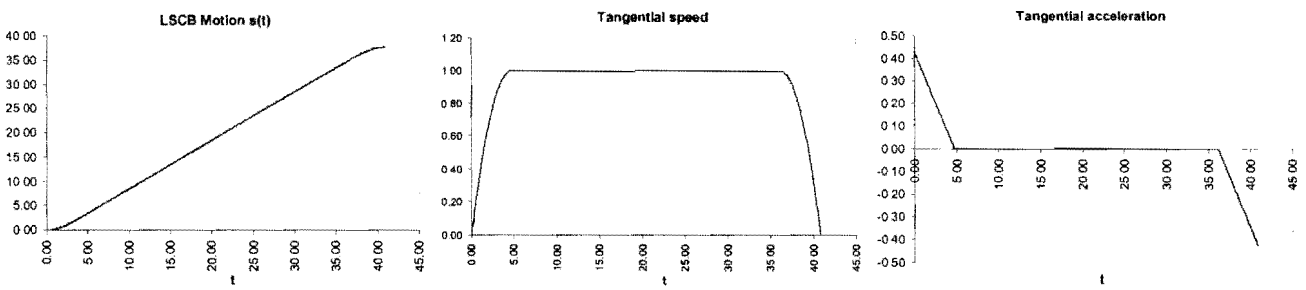

Figure 3.29: LSCB-motion for the circular curve with its accompanying speed and acceleration curves.

Figure 3.30 shows the x- and y-positions $X(t)$ and $Y(t)$ (with start point $(3,0)$ at $t = 0$ and end point $(3,0)$ at $t = 40.841\,s$), the x- and y-velocities $\dot{X}(t)$ and $\dot{Y}(t)$ (designated as Vx and Vy), and the x- and y-accelerations $\ddot{X}(t)$ and $\ddot{Y}(t)$ (designated as Ax and Ay) over the time interval $[0, 40.841]$.

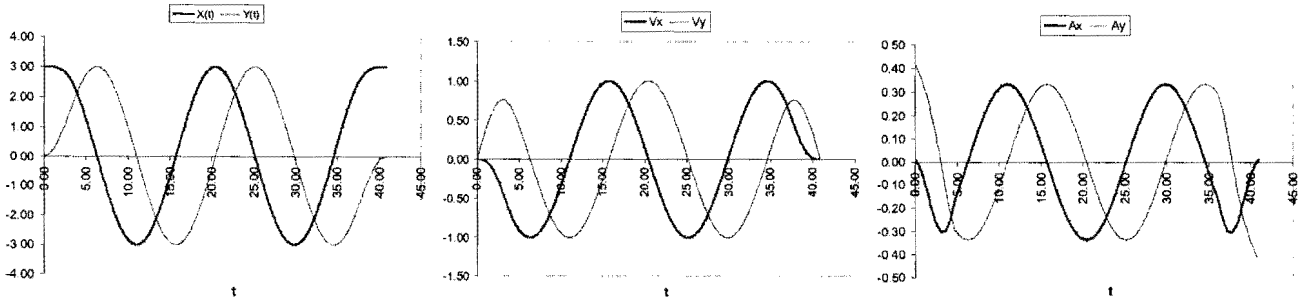

Figure 3.30: Plots of the approximate coordinates, velocities and accelerations versus time for the circular curve.

For the circular test curve, the situation depicted in Figure 3.14 occurs, where the specification of a tangentially orientated end-effector necessitates the monitoring of the behavior of the *calculated gradient angle* θ to keep track of the end-effector *orientation angle* ϕ (see Section 3.4). The corresponding cubic spline approximation $\Phi(t)$ [degrees] that results from the monitoring procedure outlined in Section 3.4 is shown in Figure 3.31. Since the nodal points were specified within the sweep angle range of $[0°,720°]$, the *orientation angle* varies from $-90°$ to $630°$. The corresponding orientation angular velocity curve $\dot{\Phi}(t)$ [rad/s] and the orientation angular accelerations $\ddot{\Phi}(t)$ [rad/s^2] are also shown in Figure 3.31.

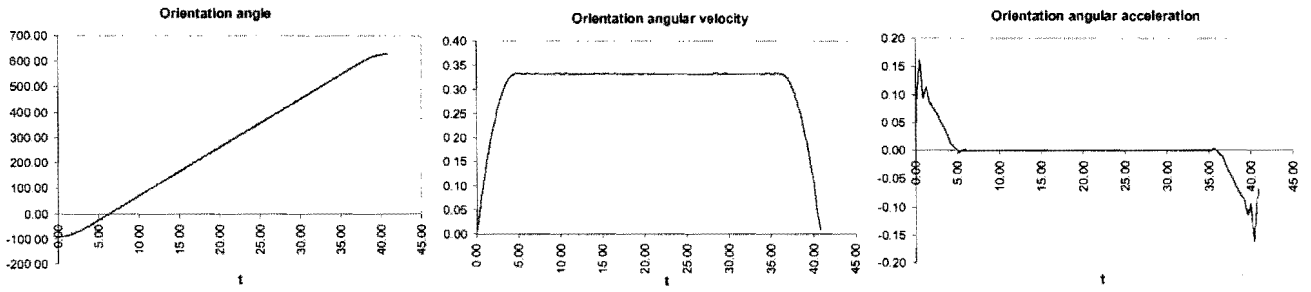

Figure 3.31: Plots of the approximate orientation angle, orientation angular velocity and orientation angular acceleration versus time for the circular test curve.

The unexpected spikes at the beginning- and endpoints of the angular acceleration curve, as opposed to the smooth behavior of both $\ddot{X}(t)$ and $\ddot{Y}(t)$ in the same regions, are probably due to the slight inaccuracies introduced in the calculation of the gradient angle via expressions (3.60) and (3.61). Expression (3.60) uses the *approximated* gradient, while expression (3.61) uses the *approximated* x- and y-velocities to find the gradient angle θ.

For the circular test curve under consideration, the exact gradient angle θ (and orientation angle ϕ) corresponding to a given *sweep angle* β may be determined (see Figure 3.32).

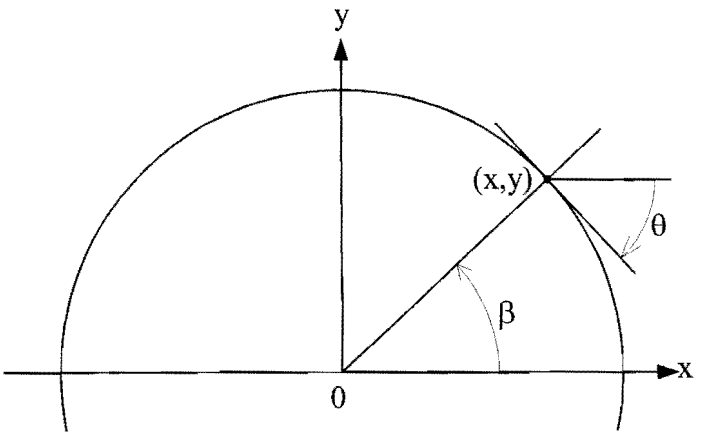

Figure 3.32: Exact gradient angle for a given sweep angle.

The figure clearly shows that the relationship $\tan\beta = \frac{y}{x}$ applies, from which it follows that the exact gradient angle is $\theta = \beta - 90°$, which also allows for the exact determination of ϕ. With this information available a comparison can be made between the approximated and exact orientation angle at any point along the curve.

Corresponding to the determination of the absolute radius error, the absolute difference between the *approximated* orientation angle, and the exact orientation angle is referred to as the orientation angle error. For the circular test curve, the maximum absolute orientation angle error over all the 781 division points is 5.714×10^{-4} rad, i.e. $0.03274°$ with an average error 3.742×10^{-5} rad, i.e. $0.00214°$.

3.5.4 Logarithmic spiral test curve

The final analytical test curve is the logarithmic spiral taken from [69]:

$$\rho = e^{0.1\beta} \tag{3.69}$$

which specifies the relationship between the polar coordinates (ρ, β) of any point on the curve.

As in the case of the circular curve of Section 3.5.3, the spiral curve can also not be expressed as a function of one coordinate variable in terms of the other. The nodal points $\{P_i = (x_i, y_i), i = 0,1,...N\}$ are generated via (3.69) where the polar angle plays the role of a sweep angle β_i. For the spiral test curve the sweep angle ranges from $-\pi$ to -5π, i.e. $\beta \in [-\pi, -5\pi]$. Note that the sweep angle is incremented such that the logarithmic spiral curve is traced in a CW manner, as opposed to the CCW-tracing of the circular test curve (see Section 3.5.3). The 79 nodal points specified are shown in Figure 3.33

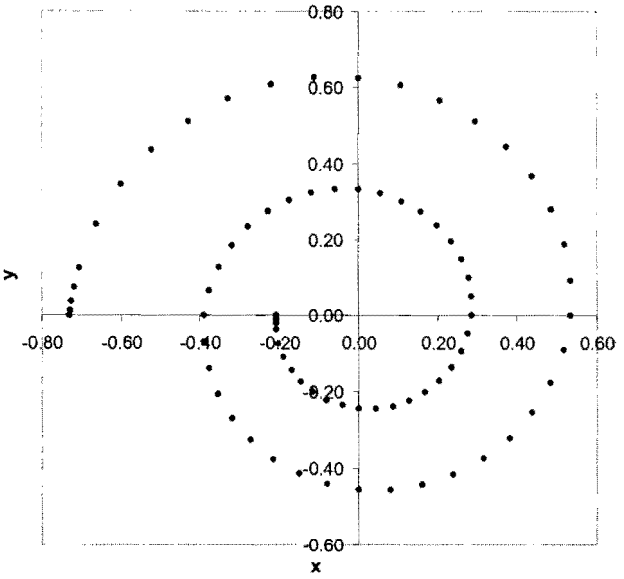

Figure 3.33: Nodal points used to approximate the spiral test curve.

Using the same procedure as outlined before, the x-y profile may be mapped at 781 division points as shown in Figure 3.34. For each interpolated point the x and y coordinates yield an interpolated radius, i.e. $r = \sqrt{x^2 + y^2}$. Furthermore, for each interpolated point the relationship $\tan\beta = \frac{y}{x}$ applies as it does for the circular test curve (see Figure 3.32). The calculated β-angle is used in a special procedure similar to the one explained in Section 3.4, to determine the exact β-polar coordinate associated with the interpolated point. Hence, by substituting the exact β-polar coordinate into expression (3.69), the ρ-polar coordinate as well as the absolute radius error $|\rho - r|$ associated with the interpolated point may be determined. The maximum absolute radius error for the spiral test curve over the 781 division points is 1.361×10^{-5} with average error 7.258×10^{-7}.

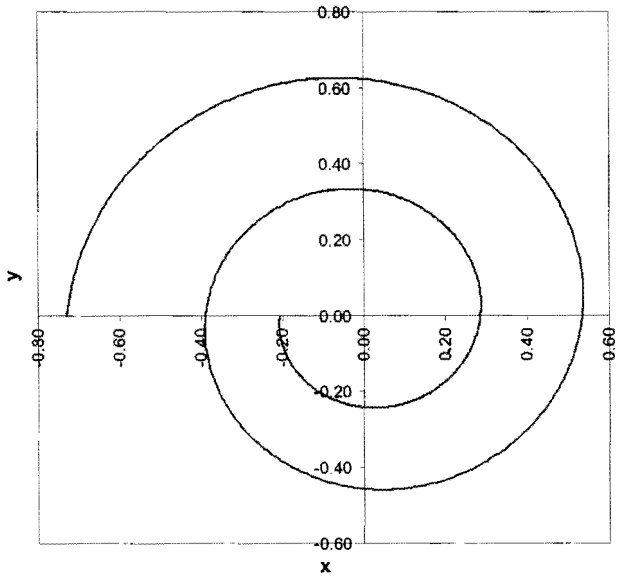

Figure 3.34: OCAS-approximation of spiral test curve.

Here the bound on the maximum allowable acceleration is 0.7 meter per second square, and a central speed of $v^* = 1\,m/s$ is specified. The resulting LSCB motion is shown in Figure 3.35, for which the respective blend times are $T_I = 2.968\,s$ and $T_{II} = 4.275\,s$ with total path time $T_{III} = 7.224\,s$. The tangential accelerations are within the specified limits, since $\ddot{s}_I(0) = 0.674 < 0.7$ and $|\ddot{s}_{III}(T_{III})| = |-0.678| < 0.7$.

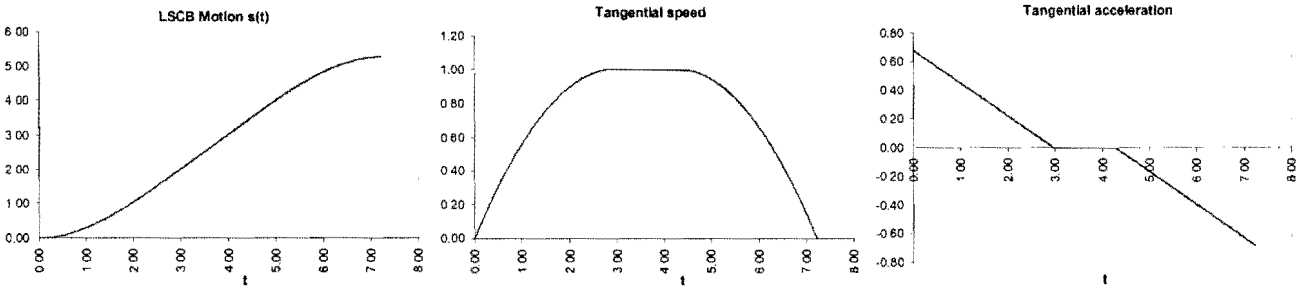

Figure 3.35: LSCB-motion for the spiral test curve with its accompanying speed and acceleration curves.

The corresponding approximated x- and y-positions $X(t)$ and $Y(t)$ (with start point $(-0.730, 0)$ at $t = 0$ and end point $(-0.208, 0)$ at $t = 7.224\,s$), x- and y-velocities $\dot{X}(t)$ and $\dot{Y}(t)$ (designated as Vx and Vy), and x- and y-accelerations $\ddot{X}(t)$ and $\ddot{Y}(t)$ (designated as Ax and Ay) computed at the 781 division points are plotted in Figure 3.36.

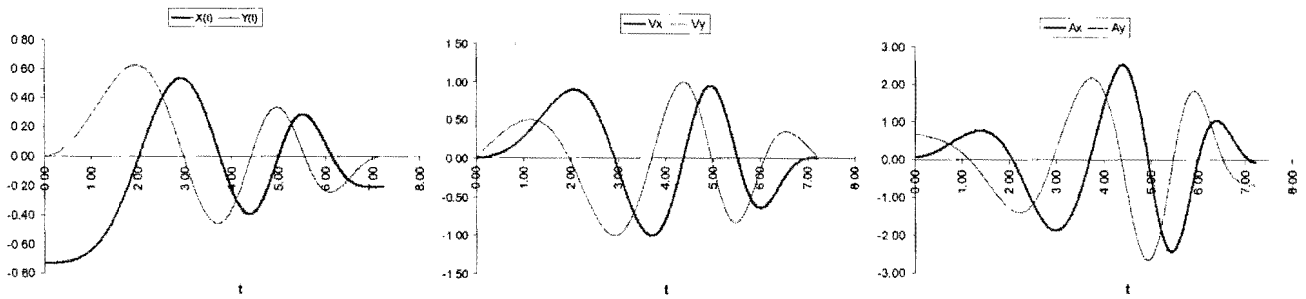

Figure 3.36: Plots of the approximate coordinates, velocities and accelerations versus time for the spiral test curve.

As for the circular test curve, the orientation angles of the spiral test curve are determined using the monitoring procedure outlined in Section 3.4. The end-effector orientation angle of the spiral test curve varies between $84.29°$ and $-635.71°$ as shown in Figure 3.37.

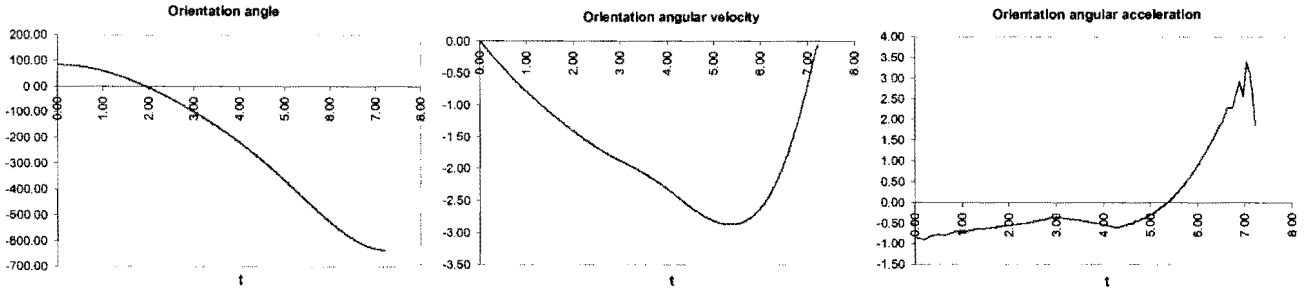

Figure 3.37: Plots of the approximate orientation angle, orientation angular velocity and orientation angular acceleration versus time for the spiral test curve.

The orientation angular velocities [rad/s] and the orientation angular accelerations [rad/s^2] are also shown in Figure 3.37. Again the spikes at end point of the angular acceleration curve are probably due to slight inaccuracies in the determination of the orientation angle (see Section 3.5.3).

Although specifying an angular offset $\phi_{offset} = -45°$ shifts the orientation angle curve *down* as shown in Figure 3.38, the orientation angular velocity and orientation angular acceleration curves remain unchanged. In particular, the *offset* orientation angle of the spiral test curve varies between $39.29°$ and $-680.71°$.

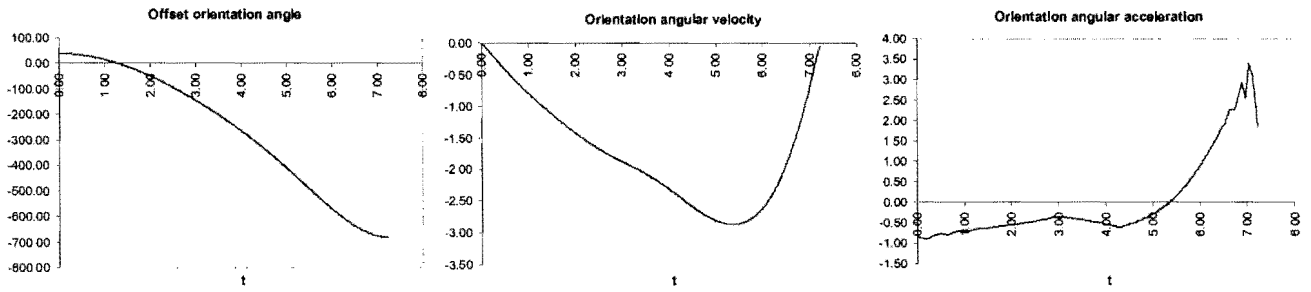

Figure 3.38: Plots of the approximate offset orientation angle, orientation angular velocity and orientation angular acceleration versus time for the spiral test curve.

3.5.5 Non-analytical test curve

The final test curve is the non-analytical treble clef shown in Figure 3.39. The particular curve is a Non-Uniform Rational B-Spline (NURBS) generated with commercial Computer Aided Design (CAD) software, and fitted through the 42 nodal points also indicated in Figure 3.39. For trajectory planning purposes, the start- and end points are as indicated in Figure 3.39.

This illustrative example is typical of a real life situation where the prescribed curve is an arbitrary smooth curve for which no analytical expression exists.

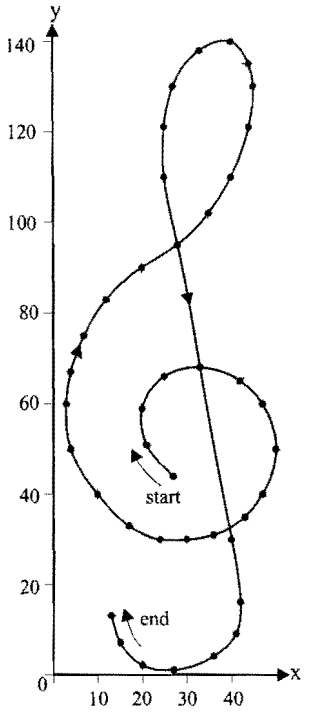

Figure 3.39: CAD-spline drawing through specified points of the treble clef test curve.

The OCAS trajectory planning methodology is tested by specifying different sets of nodal points, where the nodal points of each set are differently spread along the CAD spline treble clef. In particular, three different sets of nodal points are chosen with respectively 22, 31 and 49 nodal points. The approximated OCAS x-y profiles computed at respectively 211, 301 and 481 division points are shown in Figure 3.40.

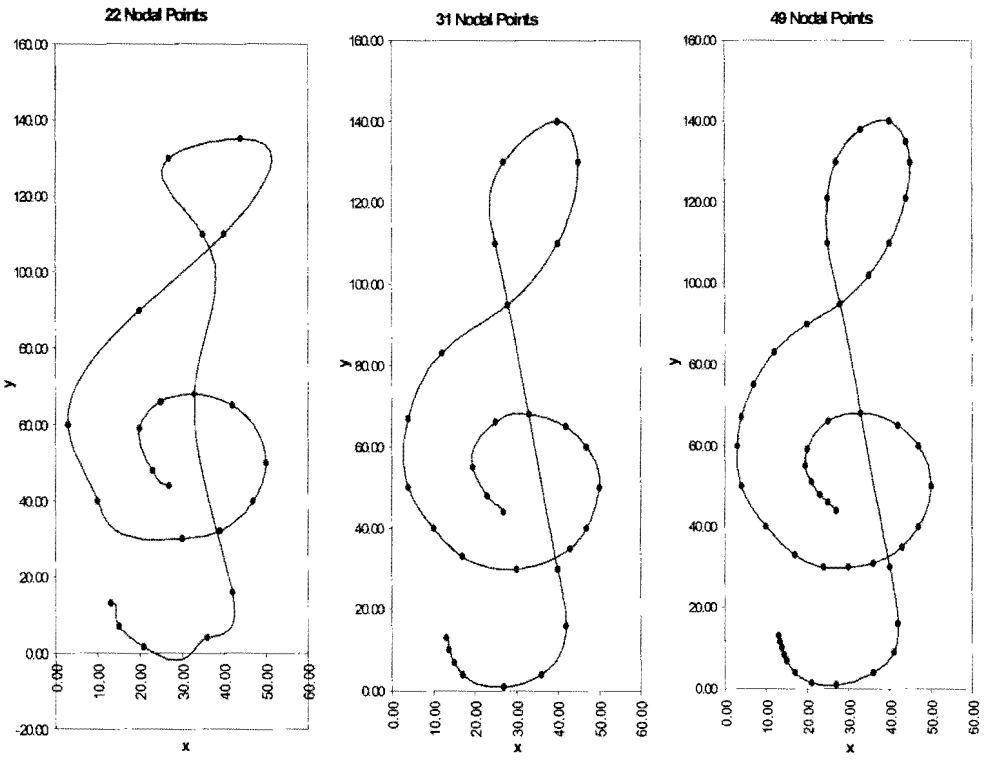

Figure 3.40: Three OCAS approximations of treble clef test curve.

By comparing Figure 3.40 with Figure 3.39, it is evident that the approximation capability of the OCAS trajectory planning methodology is accurate with relatively few specified nodal points. Using only 31 nodal points yields a reasonably accurate fit, while using 49 nodal points yields an approximation which by inspection shows no deviation from the original CAD-spline treble clef. However, specifying too few nodal points, and in an injudicious manner, results in a poor approximation as can be seen from the x-y profile computed for the 22 chosen nodal points in Figure 3.40.

The results presented in Figure 3.40 also emphasize the importance of clustered distributions of nodal points near the extreme points (especially the end point) of the prescribed curve, which ensure accurate approximations to $\frac{dy}{dx}$ at P_0 and P_N.

Since the choice of 49 nodal points gives the best approximation, its associated trajectory planning results are also shown. Here the bound on the maximum allowable acceleration is $5\,mm/s^2$, and a central speed of $v^* = 10\,mm/s$ is specified. The resulting LSCB motion is shown in Figure 3.41, for which the respective blend times are $T_I = 5.126\,s$ and $T_{II} = 40.1435\,s$ with total path time $T_{III} = 44.693\,s$. The tangential accelerations are within the specified limits, since $\ddot{s}_I(0) = 3.834 < 5$ and $|\ddot{s}_{III}(T_{III})| = |-4.396| < 5$.

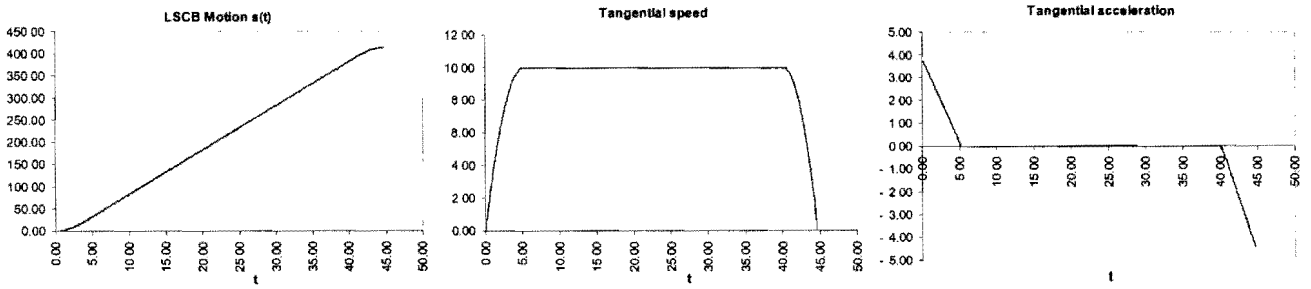

Figure 3.41: LSCB-motion for the treble clef test curve with its accompanying speed and acceleration curves.

The corresponding approximated x- and y-positions $X(t)$ and $Y(t)$ (with start point $(27.0, 44.0)$ at $t = 0$ and end point $(13.0, 13.0)$ at $t = 44.693\,s$), x- and y-velocities $\dot{X}(t)$ and $\dot{Y}(t)$ (designated as Vx and Vy), and x- and y-accelerations $\ddot{X}(t)$ and $\ddot{Y}(t)$ (designated as Ax and Ay) computed at the 481 division points are plotted in Figure 3.42.

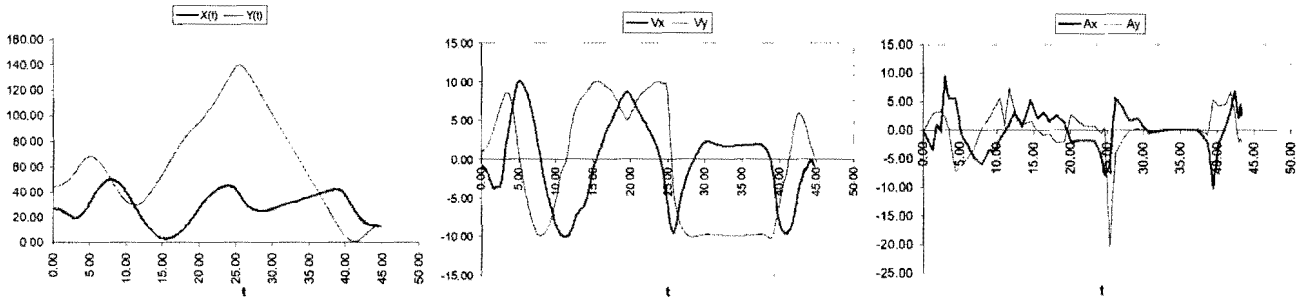

Figure 3.42: Plots of the approximate coordinates, velocities and accelerations versus time for the treble clef test curve.

The treble clef prescribed curve is traced with the end-effector in a fixed horizontal orientation $\phi = 0°$, hence the orientation angle curves are omitted here.